Simulation of temperature and stress during and after RCC dams construction

M. Cervera
M. Goltz

Monograph CIMNE Nº-76, September 2003

Simulation of temperature and stress during and after RCC dams construction

M. Cervera
M. Goltz

Monograph CIMNE Nº-76, September 2003

INTERNATIONAL CENTER FOR NUMERICAL METHODS IN ENGINEERING
Gran Capitán s/n, 08034 Barcelona, Spain

INTERNACIONAL CENTER FOR NUMERICAL METHODS IN ENGINEERING
Edificio C1, Campus Norte UPC
Gran Capitán s/n
08034 Barcelona, Spain
www.cimne.upc.es

First edition: September 2003

SIMULATION OF TEMPERATURE AND STRESS DURING AND AFTER RCC DAMS CONSTRUCTION
Monograph CIMNE M76

ISBN: 84-95999-34-X

Depósito legal: B-40322-2003

Contents

List of Figures

List of Tables

Notation

The following symbols are used in this diploma thesis:

A_f, B_f = Material properties for aging evolution;
$A_\xi, A_{\xi 0}$ = Chemical affinity, Initial chemical affinity;
$\widetilde{A}_\xi$ = Normalized chemical affinity;
C = Heat capacity per unit volume;
$\boldsymbol{D}, \overline{\boldsymbol{D}}$ = Constitutive (fourth order) tensor; Normalized *idem*
$d^\pm$ = Compressive/tensile damage;
E, E_∞ = Elastic modulus, Final elastic modulus;
E^i = Elastic Modulus for Maxwell element i;
E_a = Activation energy;
$f^\pm, f^\pm_\infty$ = Tensile/compressive strength, Final values;
$G^\pm$ = Tensile/compressive strength, fracture energy;
k_T = Thermal conductivity;
n_T = Exponent for strength evolution;
$\boldsymbol{p}_j$ = Unit vector associated with principal direction j;
Q_ξ = Latent heat per unit of hydration degree;
Q = Hydration heat per unit volume;
$\bar{Q}_\infty$ = Final amount of liberated heat (in ideal conditions);
$\boldsymbol{Q}$ = Heat flux;
R = Contant for ideal gases;
R_{ext} = External volume heat sources;
$r^\pm$ = Normalized damage tensile/compress. thresholds;
$r^\pm_e$ = Normalized elastic tensile/compress. thresholds;
$r^\pm_p$ = Normalized peak values for tensile/compress. thres.;
T, T_0 = Temperature, Initial temperature;
T_{ref} = Reference temperature;
T_T = Maximum temperature for strength evolution;
w/c = Water/cement mass ratio;
α_T, α_ξ = Thermal and chemical expansion coefficients;
$\boldsymbol{\varepsilon}, \boldsymbol{\varepsilon}_e$ = Strain tensor, Elastic strain tensor;
$\boldsymbol{\varepsilon}^i_e, \boldsymbol{\varepsilon}^i$ = Elastic, Viscous strain tensor for Maxwell element i;
$\boldsymbol{\varepsilon}_T, \boldsymbol{\varepsilon}_\xi$ = Thermal strain tensor, Chemical strain tensor;
$\eta_\xi, \eta_{\xi 0}$ = Viscosity, Reference viscosity (ref. to ξ);
$\eta_\mu, \eta_{\mu 0}$ = Viscosity of the flow term; Initial viscosity;

$\bar{\eta}$ = Exponent for viscosity;
κ = Aging degree;
λ_E = Elastic modulus aging function;
μ = Normalized micro-prestress;
ν = Poisson's ratio;
$\boldsymbol{\sigma}, \overline{\boldsymbol{\sigma}}$ = Stress tensor, Effective stress tensor;
$\bar{\sigma}_j$ = Principal effective stress value j;
$\sigma_\mu, \sigma_{\mu 0}$ = Micro-prestress; Initial micro-prestress;
τ^i = Relaxation time for Maxwell element i;
$\tau_\mu, \tau_{\mu 0}$ = Relaxation time associated to flow term, Initial value;
ξ, ξ_{set} = Hydration degree, Hydration degree at setting;
$\xi_\infty, \bar{\xi}_\infty$ = Final hydration degree, *idem* in ideal conditions;
$\dot{(\,)}$ = Time derivative or rate;
$\mathbf{1}$ = Unit (second order) tensor;
$\boldsymbol{I}$ = Unit (fourth order) tensor;
$(\,) \otimes (\,)$ = Tensorial product;
$(\,) : (\,)$ = Doubly contracted tensorial product; and
$< >$ = Macaulay brackets.

Chapter 1

Introduction

1.1 Motivation and Background

RCC has gained world wide acceptance as an alternative to conventional concrete dam construction due to the construction advantages and proved performance. RCC construction method permits a considerable reduction of costs and construction time with aid of compaction equipment and metholo-gies normally employed for earthfill placement, while maintaining the increased safety of concrete dams.

The investigation and the evaluation of the risk of cracking in RCC dams are among the main tasks during the design and the construction phase. Even though cracking does not lead immediately to the failure of a RCC dam by loss of stability, it decreases its durability. This is due to the fact that it favors filtration and the effects of freezing and thawing. As dams are hydraulic structures, cracks can cause leakage and therefore affect their serviceability. Cracking of mass concrete is primarily associated with thermal effects. Placing transverse contraction joints or the restriction of the concrete placement temperature are measures to control thermally induced cracking in RCC dam construction. However, on one hand this measures decrease the risk of cracking, but on the other hand they increase the construction costs. They can also prolong the construction time if placement has to be stopped due to placement temperatures exceeding the restrictions. Detailed studies on the evolution of temperature and stresses in the structure may avoid unnecessary contraction joints as well as construction controls too tight.

Mass concrete structures are different from many concrete structures in that material properties have a significant effect on the stress state in the structure. These material properties are not only dependent on the type and quantity of material, but on age of the concrete, temperature of the concrete, and the stress state of the material. Furthermore, certain material

properties exhibit non-linear behavior. Consequently, rigorous analyses of the mass concrete structure have to consider the phenomena which take place in the material, like hydration, aging, damage and creep, as well as the interactions between the structure and its environment. Another source of complexity is that the RCC dams are constructed over a long period of time. Therefore thermal stresses develop during the construction phase and may be significantly affected by subsequent operation activities.

Cervera *et al.* from the International Center for Numerical Methods in Engineering (CIMNE) in Barcelona have developed a thermo-chemo-mechanical model for concrete, considering the relevant features of its behavior at early ages, such as hydration, aging, creep and damage. This model is implemented in the Finite Element program COMET (COupled MEchanical and Thermal analysis) so that it allows to perform a thermo-mechanical analysis of RCC dams taking into account the behavior of the concrete, the evolutionary construction process, and ambient conditions.

The prediction of the constitutive model regarding the thermo-mechanical behavior of concrete at early ages has been verified by simulation of various tests. Also some simulations of construction of RCC dams have been performed. Until now, analyses of the long term thermo-mechanical behavior of RCC dams have required time consuming 2-D models. The aim of this work is to modify a 1-D model in such a way that it allows to simulate the long term behavior of temperatures and stresses in the core of a dam at low CPU time costs. Results of such simulations may be used as input parameters for the 2-D or 3-D models. The modified 1-D model may be also very helpful if decisions on the construction schedule or on the placing temperature have to be made during the construction phase. In this work the predictions of the modified 1-D model are compared with the temperature data obtained from a series of thermometers which are installed in the Rialb RCC dam in order to evaluate the results. This helps also to determine the boundary conditions of the evolutionary model.

1.2 Overview

This diploma thesis is subdivided in the following chapters:

Chapter 2 describes the materials used for RCC and its properties.

Chapter 3 gives a summary of the development of RCC dams in the last 20 years. It also deals with the relevant features of RCC construction method.

Chapter 4 outlines the thermal and mechanical behavior of RCC dams.

It discusses the input parameters used in a thermo-mechanical analysis and describes the applied models.

Chapter 5 gives a brief description of the thermo-mechanical model developed by Cervera *et al.*

Chapter 6 presents the thermo-mechanical analysis of Rialb RCC dam. The real construction process and construction within 12 months are simulated.

Chapter 7 contains some concluding remarks, summarizing the major results of this work.

Chapter 2

Roller-Compacted Concrete (RCC)

The American Concrete Institute (ACI) defines RCC as "concrete compacted by roller compaction, concrete that, in its unhardened state, will support roller while being compacted". RCC is designed to meet the material strength and durability requirements established by the structural engineer. The factors that affect the properties of conventional mass concrete (CMC) such as water-cement ratio, quality of mixing ingredients, and degree of consolidation and curing, also affect the material properties of RCC. The principal difference between CMC and RCC is the mixture consistency and the method of consolidation (U.S. Army Corps of Engineers (U.S.ACE), 1993). Internal consolidation using immersion-type vibrators is used for conventional concrete, while external consolidation with spreading equipment and vibratory rollers is used for RCC. The RCC mixture proportioning procedures are similar to conventional concrete; however RCC mixtures will normally contain less water and paste and more sand to avoid segregation.

2.1 Materials

2.1.1 Cementitious Materials

Type II portland cement (this type of cement is specified by generating less heat at a slower rate and having a moderate resistance to sulfate attack) is commonly used with RCC because of its low hydration heat and its longer set times. The slower rate of strength development of some cements generally results in greater ultimate strength for a given cement content.

The use of a pozzolan or fly ash may be especially beneficial in RCC. They act as a mineral filler to improve workability, and delays final set.

Their use also contributes to lower heat generation at early ages, and reduce costs, due to replacing part of the cement. Furthermore it may increase resistance to sulfate attack, and may be capable of reducing expansion from the alkali-silica reaction.

2.1.2 Aggregates

One of the most important factors in determining the quality and economy of concrete is the selection of a suitable source of aggregate. As with conventional concrete, aggregates for RCC should meet the same standards for quality and grading. The concrete produced from the proposed materials should fulfill the requirements of the project for strength, durability, water tightness, and economy. The typical maximum size of aggregates is 75 mm. Use of larger aggregate greatly increases the probability of segregation during transporting and spreading RCC and seldom significantly reduces the RCC cost. Coarse aggregates for RCC are graded to standards identical to those for conventional mass concrete. However, the fine aggregate used for RCC will normally contain a greater proportion of material passing the 75 μm sieve in order to fulfill paste and workability requirements. RCC containing minimally processed pit run aggregate may require a greater water content, be less durable, have a lower stress, and less bond between lifts than RCC containing properly processed aggregates.

2.1.3 Chemical Admixtures

Chemical admixtures can be used to improve workability, delay time of setting and enhance durability of RCC mixtures. Due to its drier consistency larger quantities of admixtures are typically required for RCC than for conventional concrete, thus increasing the relative cost. The use of a water-reducing and retarding admixture should be considered for any RCC placement. The use of this admixtures has proven to benefit for extending workability of RCC and increasing the initial and final times of setting, thereby enabling a better bond and increasing the likelihood of a watertight joint. The extended workability is especially beneficial during warm weather, during RCC start-up activities, for transporting RCC from distant sources, and for placement of thicker lifts. It also results in a decreased water content.

2.2 Properties

The properties of hardened RCC are similar to those of conventionally placed mass concrete. Where differences exist, they are generally due to

the lower water content in RCC, differences in void content, or slight aggregate or other material differences.

2.2.1 Strength

Strength properties of RCC are heavily dependent on the degree of compaction, aggregate quality, and cementitious content. RCC differs from CMC due to the more frequent horizontal planes of weakness (construction joints) created during placement, each with tensile and shear strength generally less than that of the parent concrete. Adequate compaction is essential for all RCC. For a properly proportioned mixture, compaction is often considered sufficient if the RCC has no more than 1.5% air voids. Five percent air voids due to incomplete compaction can result in a 30% loss of strength, while 20% air voids can produce a strength loss of 80% (Kaplan, 1960). The more difficult a RCC mixture is to compact, the more likely is that incomplete compaction will occur and that strength will be less than desired. Aggregates that produce high strength are not always the ideal material for RCC dams. On some projects, the use of aggregates of lower physical strength has produced RCC with desirable creep rates, low elastic moduli and good tensile strain capacity. However, the same aggregates may also produce low tensile strength and low shear properties, that are important for structures in seismic areas. The use of significant quantities of pozzolan may result in slower strength gain but, often, higher ultimate strength. Tensile strength and shear strength at lift joints are affected by degree of compaction, aggregate quality, and cementitious content, but also by the lift joint preparation and condition. The chance of obtaining the desired bond and shear strength at lift joints is less likely with RCC mixtures that are to dry to be easily consolidated or with RCC mixtures that are designed with inadequate paste volume. Lift joint bond as well as shear strength, to a lesser degree, and the overall variation of these properties in a structure will generally be improved with the use of a bedding mortar or concrete and rapid placement of successive lifts.

Compressive strength

As with CMC, compressive strength is used as a gauge of the overall strength of RCC, as well as a gauge of other properties such as durability. It is rarely a concern for design loading. Tensile strength is generally the principal concern for design. Compressive strength can be measured during construction to monitor mixture variability, to confirm achievements of design properties, and for historical purposes. Compressive strength is primarily affected by cementitious material content, type of cementitious materials, aggregate

quality and grading, and degree of compaction achieved. Common RCC mixtures may produce compressive strength ranging from 6.9 MPa to over 27.6 MPa at 1-year age. Most RCC projects have used mixtures producing an average compressive strength between 13.8 and 20.7 MPa at 90-days to 1-year age.

Tensile strength

The tensile strength of RCC is dependent on cementitious material content, aggregate strength and bond characteristics with the paste, degree of compaction of the mixture, and lift surface condition and treatment. The tensile strength is more dependent on aggregate bond than compressive strength, hence the relationship between the tensile strength and the compressive strength of concrete not only varies with the method of test but also varies with the type and maximum size of aggregate. The ratios of tensile strength to compressive strength for RCC mixtures have typically ranged from about 5 to 15%, depending on aggregate quality, strength, age, and test method. Lift joints are the weakest locations in RCC, as in CMC, structures. Hence, the tensile strength at the lift joints is the critical tensile property for RCC. Inadequate lift surface cleanup, segregation, or poor consolidation can drastically reduce the tensile strength across lift lines. Good quality aggregates, good mixture workability and compaction effort, rapid covering of lift joints by subsequent lifts, and the use bedding mortar are required to obtain good bond strength at the joint. The mortar bedding ensures that there is adequate paste at lift surface boundary to provide bond and to fill any rock pockets at the lift surface.

2.2.2 Elastic Properties

Modulus of elasticity (E)

Properly proportioned and consolidated RCC should provide a modulus of elasticity equal to or greater than that of CMC of equal compressive strength made with similar materials. E is dependent on age, strength, and aggregate type, and the same modulus-strength relationships used for CMC may be used for RCC. Modulus of elasticity of CMC is about 6.9 GPa at 1 day and ranges from about 21 to 38 GPa at 28 days and from about 30 to 47 GPa at 1 year. Lower quality aggregates have been successfully used in RCC, often resulting in very low E at all ages. Hence, RCC values of E tend to have a wider range than for CMC. A low modulus of elasticity is generally beneficial in reducing apparent stress and strain in the structure. Low strength mixtures will generally produce low moduli.

Poisson's ratio

Poisson's ratio is defined as the ratio of the lateral to the longitudinal strain resulting from a uniformly distributed stress. Poisson's ratio for RCC is the same as for CMC. For static loads, most values range between 0.17 and 0.22.

2.2.3 Tensile Strain Capacity

Tensile strain capacity (TSC) is the change of length per unit length that can be sustained in concrete prior to cracking. Tensile strains can be developed by external loads as well as by volume changes induced through drying, reduction in temperature, and autogenous shrinkage. It is dependent on time and rate of loading, type of aggregate shape characteristics (angular as produced by crushing versus natural rounded) and is strongly dependent on strength. The Corps of Engineers introduced TSC testing of concrete to provide a basis for evaluating crack potential for strain-based thermal studies of mass concrete structures (Houghton, 1976). TSC is determined in a series of tests that include normal and slow loading of beams. The slow load test was designed to simulate the strain conditions in a mass concrete structure during long term cooling. Normal load rate tests were designed to simulate strain conditions near the surface of a mass concrete structure where cooling occurs more rapidly.

2.2.4 Volume Change

Drying shrinkage

Drying shrinkage is governed primarily by the water content of the mixture and the characteristics of the aggregate. RCC drying shrinkage is similar to or lower than that of CMC due to the lower water content of these mixtures. The effects of drying shrinkage are generally ignored for analysis of mass concrete structures, since the interior of this structures generally remains moist, except for possible application to surface cracking.

Autogenous volume change

Autogenous volume change, commonly called "autogenous shrinkage", is a decrease in volume of the concrete due to hydration of the cementitious materials without the concrete gaining or loosing moisture. This type of volume change occurs in the interior of a large mass of concrete and can be a significant factor. It is primarily related to the material properties and

proportions in the mixture and especially the type of aggregate. Autogenous shrinkage occurs over a much longer time than drying shrinkage.

2.2.5 Thermal Properties

Adiabatic temperature rise

An adiabatic system is a system in which heat is neither allowed to enter nor to leave. The adiabatic temperature rise, therefore, is the change in temperature in concrete due to heat of hydration of cement under adiabatic conditions. It is the measure of heat evolution of the concrete mixture in a thermal analysis. In very large masses of concrete, temperatures near the center of the mass will peak near the sum of the placement temperature and the adiabatic temperature rise. The magnitude of the adiabatic temperature rise and the shape of the curve can vary significantly for different concrete mixtures. Typical values for mass concrete range from 11 to 19^oC at 5 days to 17 to 25^oC at 28 days.

Specific heat

Specific heat is the amount of heat required per unit mass to cause a unit rise of temperature. It is affected by temperature changes but should be assumed to be constant for the range of temperature in mass concrete structures. Typical values range from 0.75 to 1.17 $kJ/(kg \cdot {}^oK)$.

Thermal conductivity

Thermal conductivity is a measure of the ability of the concrete to conduct heat and is defined as the rate at which heat is transmitted through a material of unit area and thickness when there is a unit difference in temperature between the two faces. For concrete thermal conductivity is calculated from the product of thermal diffusivity, specific heat, and density. Thermal conductivity of mass concrete is not significantly affected by age or by changes in temperature over typical ambient temperature ranges but is influenced by aggregate type. Typical values range from 1.73 to 3.46 $W/(m \cdot {}^oK)$.

Thermal diffusivity

Thermal diffusivity is a measure of the rate at which temperature change can occur in a material and is defined as the thermal conductivity divided by the product of specific heat and unit weight. For mass concrete, thermal diffusivity is not substantially affected by aggregate temperature or age. It is influenced by aggregate type and concrete density. Thermal diffusivity is

used to calculate thermal conductivity used for FE analysis. Typical values range from 0.003 to 0.006 m^2/h.

2.2.6 Permeability

Permeability of the RCC mass and of the horizontal lift surface are key elements for hydraulic RCC structures. The permeability of RCC is largely controlled by mixture proportioning, placement method, use of bedding mortar on lift surfaces, and the degree of compaction. Concrete with low permeability generally has a lower water-cementitious material ration, is well mixed an consolidated, is proportioned with adequate paste and mortar to sufficiently fill all voids, and has been properly cured to allow for the continued hydration of cement. High cementitious material content have lower permeability than low cementitious material content mixtures. Test values for well-compacted, workable RCC mixtures typically range from 1.5 to 150 x 10^{-8} mm/s. Measured RCC permeability values have a very large range because of the wide range of mixtures used and the wide range of density achieved in structures and test specimens due to the use of cores and cylinders specimens and the variety of permeability tests used (Dunstan, 1988).

2.2.7 Density

Density of RCC depends primarily on aggregate density and the degree of compaction. Typical values of density for RCC range from 2240 to 2560 kg/m^3. The lack of entrained air and lower water content of many RCC mixtures results in a slightly higher density when compared to conventional air-entrained mass concrete made with the same aggregates.

Chapter 3

RCC Dams

3.1 The Evolution and Development of RCC Dams

Until 1950, about 38% of the large dams, except for China, had been constructed with concrete. Between 1951 and 1977 the portion decreased to 25%, reaching a minimum of 16% during the period of 1978 and 1982. This decrease coincides with the increase of the construction of arch dams in closed valleys. In the vast valleys, embankment dams have been more competitive. But the economic advantage results in a decreased safety in comparison with concrete dams. Numerous embankment dams have suffered a failure in the last 60 years. In most cases caused by overtopping or internal erosion.

For this reason, in the last 30 years, huge efforts have been made to develop an alternative construction method, which combines the higher safety of concrete dams with the efficiency of the construction method of embankment dams. This consideration have led to the development of RCC dams.

The basic concept of RCC appeared during the forties in England for the first time, used as a subbase in highway an airfield construction. In 1970 Raphael published the article "The Optimum Gravity Dams", in which he considered to use this concept in dam construction. The rehabilitation of the Tarbela dam in Pakistan using what the consultants termed "rollcrete" was a major step forward in the development of the RCC dam (Hansen, 2000). During the initial filling of the Tarbela reservoir in 1974 one of the four 13.7 m diameter outlet tunnels collapsed (see Figure 3.1). Because repair needed to be completed before the next flood season some $350,000$ m^3 of no slump RCC were placed in 42 working days. The results obtained from Tarbela proved the rapid placement and erosion resistance of RCC.

The first RCC dams have been the 89 m high Shimajigawa dam (Figure

Figure 3.1: Collaps of outlet tunnel at Tarbela dam.

(a) (b)

Figure 3.2: (a) Shimajigawa dam. (b) Willow Creek dam.

3.2(a)), in Japan, completed in 1981, where RCD (roller-compacted dam, concrete method) was used for the interior concrete, and the 52 m high Willow Creek dam (Figure 3.2(b)), in USA, completed in 1982. The design concepts of both projects are quite different. While the engineers in the USA tried to complete their RCC dam projects with the cost of embankment dams by reducing material cost and fast placement, the idea of the Japanese concept was maintaining the same strict demands for watertightness strength and durability as for traditional mass concrete dams and using the economic benefits of the higher placement rate of RCC.

For the first ten years of RCC dam construction, that is up to 1994, the average size of a dam being completed did not changed too much. The average height of the RCC dams completed each year varied between 40 and 50 m and the average volume between $100,000\ m^3$ and $200,000\ m^3$ (see Figure 3.3). It was not until 1995 that there seemed to be sufficient confidence to increase the size of RCC dams. But while engineers in Japan have not

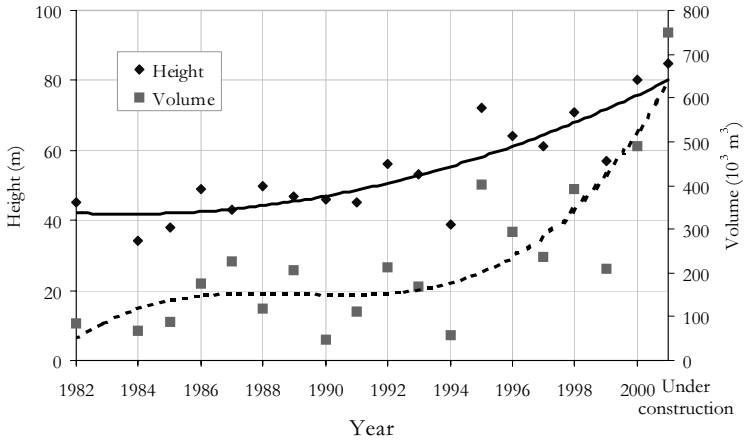

Figure 3.3: Heights and volumes of RCC dams.

changed their RCD design and construction methods since Shimajigawa, all the RCC dams in Japan are of the RCD type (Dunstan, 1999), the other leading countries in RCC dam construction (China, USA, and Spain) have learned considerably about the installation of transverse contraction joints to control thermal cracking. Especially from the Upper Stillwater dam (USA), where the first crack appeared in 1988, just about one year after construction was completed. The Upper Stillwater dam which was with a RCC volume of $1,125,000\ m^3$ the world biggest RCC dam until the completion of Guanyinge dam (China), was constructed without either contraction joints or internal mass concrete cooling. Since 1995 it is quite common to use contraction joints to control thermally induced cracking and there has been a steady increase in the size of structure. The average height of RCC dams completed in 2000 is about 80 m, and the average volume of RCC in the dam $491,000\ m^3$. The average height of the RCC dams at present construction is 85 m, and the average RCC volume $749,000\ m^3$. Among these dams are La Miel (Colombia), which will be the highest RCC dam in the world with 188 m and Tha Dan (Thailand), the world largest RCC dam with a RCC volume of $4,900,000\ m^3$. However, even these marks will be exceeded by Longtan dam in China, which will have a height of 217 m and an RCC volume of $7,500,000\ m^3$ if this project is to be built as planned.

But not only the size of dams has changed since the completion of Shimajigawa, there was also a change in the cementitious content of the RCC mixture. After the construction of the first RCC dams, which had an cementitious content between 66 kg/m^3 and 120 kg/m^3, there was a trend to higher cementitious content RCC in the following years. This change stabilized in 1992, and since then, the proportion of dams being completed

using the various different design philosophies (Dunstan, 1989) remained relatively stable, as follows (Dunstan, 1999):

High-paste content RCC dams (cementitious content > 150 kg/m^3)	45±2 %
Medium-paste RCC dams (cementitious content 100 to 149 kg/m^3)	23±2 %
RCD dams (as constructed in Japan)	16±2 %
Lean RCC dams (cementitious content < 99 kg/m^3)	12.5±1.5 %
Hardfill dams (Londe and Lino, 1992)	1.0±0.5 %

It seems, that the compound of the RCC mixture concerning the cementitious content is adapted to the demands and conditions of the constructing country. In Brazil, for instance, where there is little or no dynamic loading and few sources of pozzolan the content of cementitious material in the RCC mixture varies between 55 to 80 kg/m^3 of cement and 0 to 30 kg/m^3 of pozzolan. Or Japan with his RCD method which is suitable for the high dynamic loading. This method uses either 120 or 130 kg/m^3 cementitious content (with one exception: Chiya dam with an cementitious content of 110 kg/m^3), depending on the height of the dam. There is also less distinction in the proportion of cement and pozzolan. The 130 kg/m^3 mixture consist of 91 kg/m^3 cement and 39 kg/m^3 low lime fly ash, and the 120 kg/m^3 mixture consist of 96 or 84 kg/m^3 cement and 24 or 36 kg/m^3 low lime fly ash.

Though of the 210 RCC dams in operation only 12 have a different cross-section than that of the traditional gravity dam, the RCC method is also suitable for other types of concrete dams. Of those that do not, five are arch-gravity dams, three in South Africa and two in China, four are arch dams, all in China and three are small hardfill dams. The construction of the 50 m high Knellport dam (South Africa), completed in 1988 and the 70 m high Wolwedans dam (South Africa), completed in 1989, was the first attempt to use the RCC technique for other shapes than the traditional gravity shape. The most important design requirement in this projects was to provide the dams with crack-inducing systems which included joint grouting facilities that would first ensure radial crack joint development at designed positions and also, to allow grouting of fully developed crack joints. The grouting produced the arch effect (Geringer, 1994). The other three arch gravity dams do not have groutable joints. Here, the designers relied on the placement in cold weather and/or the movement of the arch to produce the arch effect. Because the performance of arch gravity dams and arch dams highly depends on the position and type of joints, thermal analysis of

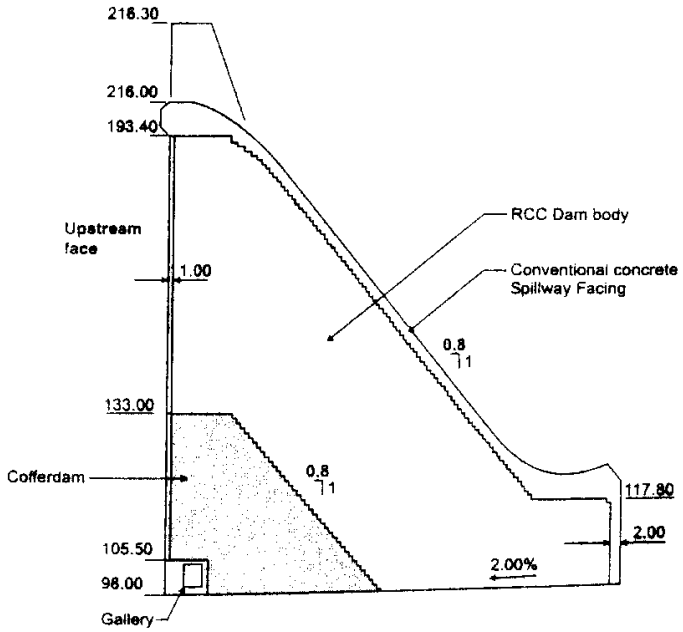

Figure 3.4: Cross-section of Beni Haroun dam.

the structures is essential. Today's techniques for thermal analysis makes it possible to design and construct large arch-gravity and arch RCC dams where the shape of the valley and the foundation, are suitable.

Another innovation in RCC dam design was the use of RCC cofferdams. The benefits of RCC cofferdams are their rapid construction and their higher resistance of erosion. They can be overtopped various times without loosing their stability. The design at Beni Haroun showed another advantage of the RCC cofferdams. There, the 35 m high cofferdam, with an RCC volume of $220,000\ m^3$, was incorporated within the base of the upstream face of the dam (see Figure 3.4).

3.2 Construction Methods

3.2.1 General Considerations

RCC dams have gained acceptance worldwide in a relative short time due to their economic advantage combined with the long-term safety record of concrete dams. One of the cost-saving features of RCC is the rapid rate at which it can be placed and consolidated by earthmoving and compaction equipment. Generally, as with most other construction processes, the faster the placement is made, the less expensive the RCC becomes. In case of a

dam, the faster placement will mean less time between placement of lifts, resulting in lift joints with improved strength and seepage performing. The potential of rapid placement also provides the designer the option of limiting placement to specific time periods to take advantage of cool or warm weather to aid in controlling the temperature of the RCC. It also provides the opportunity to reduce the extent of cofferdam and diversion requirements.

3.2.2 Transportation Systems

The mixed RCC is transported to the placement area either by conveyor belt, by conventional batch and houl methods, or by a combination of both. As the quality of lift surface is affected by the process used to transport the material to the placement site, choosing the transportation system not only depends on the volume of the concrete to be placed or the costs. In general, high-quality lift surfaces, particularly those requiring high lift strength, are better constructed using conveyor belts for transportation on the dam (U.S. Army Corps of Engineers (U.S.ACE), 2000). Employing conventional batch and haul methods care must be taken to assure that transportation vehicles do not track dirt or mud onto the RCC placement, and that segregation does not occur prior to final compaction of the RCC. The high daily placement rates of RCC, which have reached as high as $10,000\ m^3$ in the recent completed RCC dams and the projects now under construction, demands a continuous transport of RCC, which can only be guaranteed by a system of conveyor belts. Figure 3.5 shows RCC being transported to the placement site.

3.2.3 Placement Procedures

Once the RCC has been transported to the placement area it is spread and leveled by dozers. Lift thicknesses can vary between 150 mm and 1 m, although lift placements of 300 mm are most common in RCC dams. Because placing the RCC in lanes must be avoided the material is advanced across the length of the dam for the full upstream-downstream dimension. The dozers work continuously so that all surfaces of the RCC layers receive at least two passes of the dozer. In this manner the RCC will be nearly completely consolidated by the action of the dozers and provide a uniform surface without ruts, bellies and humps. Areas in which segregation occurs are removed and respread with fresh RCC. Additional layers of RCC are spread until the final lift thickness is achieved and final compaction rolling begins. Figure 3.6(a) shows an RCC-placement operation.

Final compaction is accomplished using vibratory roller compactors.

Figure 3.5: Transporting RCC by conveyor belt.

Typically, four to six roller passes are adequate to achieve desired densities for RCC lifts of 300 mm thickness. It should be noted that excessive rolling can actually decrease the density of some mixtures. After final rolling the compacted RCC surface must be kept clean and continuously moist until placement of the next lift. Because excessive time intervals between placing and compaction reduce the strength of the structure these intervals must be kept small. Figure 3.6(b) shows RCC compacted by vibratory roller.

3.2.4 Lift Surfaces

Lift joints or horizontal construction joints are formed at the interface between successive RCC lifts. The total number of lift joints in an RCC

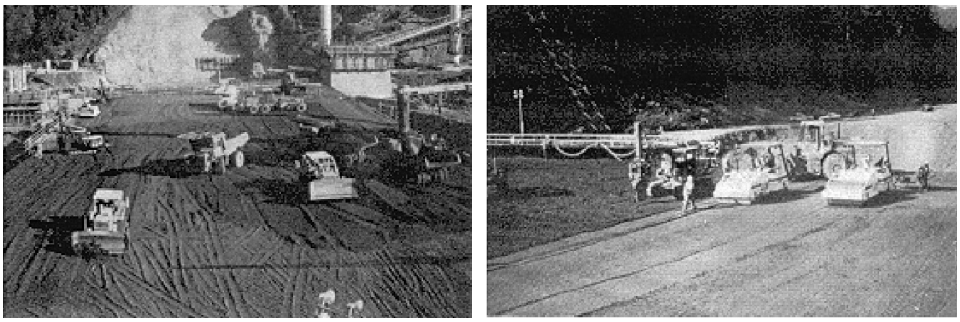

(a) (b)

Figure 3.6: (a) RCC-Placement operation. (b) Compaction by vibratory roller.

structure is determined by the thickness of each lift and the overall height of the structure. Tensile and shear strength at lift joints are less than in the parent RCC. Segregation of the RCC and lack of bond at the lift joints often result in increased seepage. Therefore lift joint surface treatment is dependent on the required bond and watertightness of the structure. Standard lift joint treatment include simple moist curing, cleaning contaminated areas by washing and vacuuming, and application of a bedding mortar or bedding concrete immediately prior to placing the next lift. Because the loss of bonding capacity at the joints begins almost immediately after placing, horizontal lift joint surfaces must be left exposed for a minimum amount of time.

The joints can be classified either as cold joints or hot joints. Theoretically a hot joint is the lift joint in which one lift is placed after another before setting of the concrete starts; all joints which do not fulfill this condition are called cold joints (Marsellá, 1996). An RCC cold joint may occur at any horizontal lift surface that is allowed to dry, set, or become contaminated prior to receive the next lift. Environmental conditions such as heat, humidity, and wind, which contribute to the drying of the surface, are significant factors in reducing the strength of the lift joint. Therefore the criterion used to determine if a lift surface is a cold joint is a combination of time and weather conditions. Though it does not exist a exact value for this criteria, joints that are 600 to 800^oC-hours or more old should be treated as cold joints (for non retarded cement mixes) (Schrader, 1999). Vertical cold joints occur when placement of the RCC is stopped or interrupted before an entire lift is complete.

RCC cold joints require special treatment in order to assure adequate bonding with the successive lift. Typical cold joint treatment include high pressure washing or wet sand blasting to remove mortar coatings, or other contaminants, followed by a high volume, low pressure washing and vacuuming to remove all excess water and debris. The surface is then maintained in a damp condition and covered with a thin layer of mortar or concrete bedding mix immediately before placing the next lift of RCC.

3.2.5 Joints and Cracking

Cracking of mass concrete due to thermal volume change may occur both in CMC and in RCC dams. Although vertical contraction joints facilitate placement in CMC structures, they do not favor the construction process of RCC dams due to the abutment-to-abutment method of placement. To avoid potential interruption of RCC production and to reduce cost the designers of the first RCC dams did not use vertical joints. However, in some of these dams significant cases of cracking occurred (Hansen and Reinhardt,

1991):

1. Copperfield dam (Australia, completed in 1982) - A transverse crack through the spillway section of the dam occurred 7 months after initial filling.

2. Galesville dam (USA, completed in 1985) - Seven significant transverse thermal cracks occurred through the dam, requiring treatment to reduce seepage.

3. Upper Stillwater (USA, completed in 1987) - Transverse thermal cracking was expected in this dam, and a number of cracks developed, several of which were significant and required treatment due to heavy leakage.

Today, placing vertical transverse joints in dams constructed with RCC is the primary consideration for control of thermal cracking. The joints are formed by inserting steel or plastic sheets, or any other bond breaker material, into the full thickness of the uncompacted RCC lift. The plates or sheets are placed adjacent to each other end to end from the upstream to downstream face to form a bond breaker that serves as a contraction joint. The contraction joint plates should be installed in every lift of RCC so that the full vertical section at the joint has the bond breaker plates. Normally, contraction joint spacing will range from 20 to 30 m. Figure 3.7 shows a contraction joint being installed.

3.2.6 Innovations

Grout enriched RCC face

This is a method for producing an upstream face that is watertight, erosion resistant and attractive while not excessively costly. No less than 14 different types of upstream faces have been utilized on RCC dams worldwide (Hansen, 2000). The system that has been used to the greatest extent is formed conventional concrete where the interface between the slump concrete and the RCC is vibrated together. This or any other system can add considerable cost to an RCC dam, especially a small dam where the conventional concrete face is a greater percentage of the total volume of concrete. Both conventional concrete and RCC contain the same basic materials, portland cement, a pozzolan aggregate and water. The main difference is that there is less cement and water in the RCC mixture. By definition, cement plus water is a grout. The concept behind Grout enriched RCC is to add grout to uncompacted RCC at the upstream face and to vibrate the grout into the RCC to produce a mixed-in-face conventional concrete face.

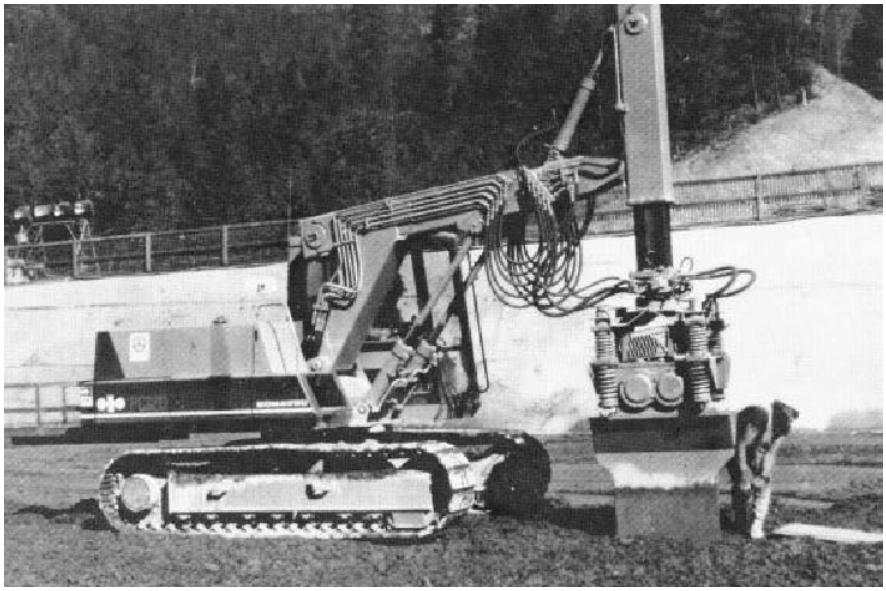

Figure 3.7: Contraction joint installation.

Sloping layer method

The sloping layer method (SLM) is a way of improving the bond between successive lifts by minimizing the time it takes to cover the previous lift. In a wide valley, too much time would pass if single 30 cm thick successive RCC lifts were placed from abutment to abutment. Chinese engineers determined that by breaking the dam into 3 m thick vertical sections and then working on slopes between $10H : 1V$ and $10H : 1V$ they could get back atop the next lift within two hours while RCC below was still alive. Improved bond thus resulted. Then the surface of the 3 m section was treated as a cold joint and a mortar bonding mix was applied every 3 m rather than every 0.3 m, thus potentially eliminating 90% of the lifts covered entirely or partially by bedding mortar.

Chapter 4

Analysis of Dams

4.1 Introduction

RCC dams have now been constructed in areas of high temperatures, low temperatures and heavy rainfall. For example, RCC has been placed at the 121 m-high Beni Haroun dam in Algeria (RCC volume = 1,600,000 m^3) with temperature as high as 43^oC. At the 91 m-high Upper Stillwater dam in USA (RCC volume = 1,125,000 m^3) and the 40 m-high Lac Robertson dam in Canada (RCC volume = 28,000 m^3), the air temperature drops to -35^oC or lower in winter. At the 113 m-high Pangue dam in Chile (RCC volume = 660,000 m^3), during the 13 months of RCC placement there was 4,436 mm of rain (including one three-month period in which 3,130 mm of rain fell while placement continued). Thus with the completion of 60 m-high Tannur dam (RCC volume = 250,000 m^3) in Jordan, in March 2001, RCC dams will have been constructed in practically all climatic conditions and in all parts of the world.

An international investigation made by ICOLD (1983) shows that there is a large number of dams with damages caused by thermally induced stresses, both during the time of construction and during their service life. The same results are obtained by a national investigation done in Spain (Aguado and Agulló, 1991), which states that about 20 to 25% of the damages observed in dams is caused by thermal effects.

The evolution of temperature in a RCC dam depends on numerous factors, which can be split into three groups:

1. The ambient conditions.
2. The (thermal) properties of the concrete mixture.
3. The construction process.

In order to avoid thermally induced cracking, it is necessary to coordinate the placing program and the consistency of the RCC mix with the local ambient conditions. With the advanced computer techniques nowadays available for thermal analysis, it is possible to perform a simulations of the thermo-mechanical behavior of a dam, which takes into account the various parameters.

4.2 Thermal Behavior of RCC Dams

Hydration of concrete is a highly exothermal process due to the large amount of hydration heat produced during the reaction. Nevertheless this heat does not cause problems in conventional concrete structures due to high dissipation and low grade of hyperstaticity during construction.

In the case of RCC dam construction the problem is different. The high concrete placement rate may lead to significant temperature rises in the entire mass. Under normal conditions some heat will be lost at the surface while the heat generated at the core is trapped. As the temperature in the core continues to increase, this concrete begins to expand. At the same time, the surface concrete is cooling and therefore, contracting. In addition, the surface may also be drying which will cause additional shrinkage. As a result of the differential temperatures and shrinkage between the core and the surface, compression develops in the interior, and tensile stresses develop at the surface. When these tensile stresses exceed the tensile strength capacity, the concrete cracks. Over a period of time the compressive stresses that are generated in the center tend to be relieved as a result of the creep properties of the material. As this is happening, the massive core also begins to cool. Over a period of several months to several years the dam cools to some stable temperature, around the average annual temperature, or a stable temperature cycle. The low thermal conductivity of the material, differential effects due to the evolutionary construction process may generate considerable thermal gradients. These, together with geometrical aspects, may develop relatively important tensile stresses (Cervera *et al.*, 2000a). As in the previous case, once these tensile stresses exceed the tensile strength capacity of the concrete, the structure will crack.

The ideal condition to avoid thermal induced cracking would be simply to eliminate any temperature gradient or temperature drop. This is possible only if there is no heat dissipation on the faces and the initial placement temperature of the concrete is set low enough so that the temperature rise due to hydration of the cement would just bring the concrete up to its final stable state.

However, it is almost impossible to provide this conditions in any dam

project; therefore other techniques must be used to control thermal stresses. Fortunately, the RCC dam construction method is advantageous in temperature control due to the following:

1. The placement of thin lifts allows for heat losses by convection and radiation.

2. The placement of concrete at constant speed and with regularity helps to produce smooth temperature gradients within the dam body.

Other measures to control temperature are using low cementitious content in the mixtures, supervising placement temperature and methods of precooling and postcooling.

4.3 Thermal Induced Cracking in RCC Dams

Every material changes its volume when its temperature changes, and thermal stress is therefore induced by the restraint of volume change. Expansion by heat generation during hardening does not always bring thermal stress even if restrained, because of low elasticity and large creep of concrete at early ages. In contrast with that, contraction of concrete by temperature drop is transformed into tensile stress by the restraint of volume change, due to higher elasticity. There are two restraints of volume change, external and internal restraint.

External restraint is caused by foundation rock or already hardened concrete below newly placed concrete. Tensile stress is induced when the concrete cools down from his maximum temperature to a stable temperature. External restraint is determined by the ratio of modulus of elasticity between concrete and foundation rock (E_C/E_R) and by the ratio of height to length of placed concrete (ACI Committee 207.2R-90, 1990). For dams constructed without any large interruption of the placement process, external restraint is restricted at its lower part, namely 1/3 to 1/4 of the dam height (Fujisawa and Nagayama, 1985). This means that a larger temperature drop is allowable for external restraint at the upper part of dams than at the interface of the foundation rock. Already hardened concrete produce in general higher restraint to the successive lifts than the foundation does. Therefore long interruptions in the placement schedule should be avoided. Cracks caused by external restraint, if fully developed, can separate the structure into discrete sections. In dams where transverse contraction joints are placed very wide, this cracking can be longitudinal or parallel to the axis of the dam.

Internal restraint is the mutual restraint of different volume changes when different areas of concrete have different temperature change. Internal

restraint always exists for any temperature change because no temperature change is uniform. Thermal stress by internal restraints is determined not by the temperature change of the considered point but by the relation to surrounding temperature change, *i.e.*, tensile thermal stress is induced if the temperature does not drop or even rises, when the surrounding temperature rise is much larger. Thermal stress by internal restraint is induced at many stages, for example when the surface and the inside of newly placed concrete experience a different temperature rise during hydration. But it is most significant when mass concrete is gradually cooled from its surface or is cooled rapidly by abrupt change of ambient temperature. These thermal stresses can cause cracking at the exterior face. Surface cracking may not cause great concern if cracking is localized, but this cannot be assumed *a priori*. Once a crack is initiated, the energy required to propagated crack is much less than the energy required to initiate a crack.

Placing transverse contraction joints is one of the methods to control cracking. The idea is to produce cracks artificially at predetermined locations and treat them later.

4.4 Thermal Analysis

The thermal analysis generates the temperature or temperature histories for the RCC dam, which are possible scenarios of thermal loadings during construction and subsequent cooling. It should account for the environmental conditions at the site, the geometry of the structure, the properties of the concrete, the construction conditions, and it should provide a basis for comparing thermal generated stresses with the strength of the concrete. The analysis may also need to account for the non-linear behavior of the concrete, the interaction of the structure and the foundation, and the effects of sequential construction and thermal gradients.

The temperature calculation requirements for the thermal analysis may range from quite simple step-by-step integration techniques (Carlson, 1937) to reasonably complex models implemented in a FE-program.

4.4.1 Input Properties and Parameters

Data collection for the thermal analysis includes acquiring information on ambient weather conditions, concrete properties, and construction parameters. The following are descriptions of these data requirements.

Ambient weather conditions

Climatological conditions. The effect of the annual ambient temperature cycle on placement temperatures, short-term and long-term cooling rates, foundation temperatures, and potential starting dates for construction must be considered. Weather data can be acquired from the national meteorological institute, from airport or other local weather station, or from project weather stations. The data usually contain daily, monthly, and annual average temperatures, as well as maximum and minimum daily and monthly temperatures. Depending on the project site location, site weather conditions may depart significantly from even local weather stations. In this case, adjustments of data from the nearest recording stations to the site can be used to estimate site temperature. The rule-of-thumb that is for every 76 m of elevation increase, there is about a 0.5^oC decrease in temperature. Temperature cycles used in thermal analysis may include (U.S. Army Corps of Engineers (U.S.ACE), 1997):

1. The normal annual temperature cycle,that is a sinusoidal-like variation of temperatures for a locale obtained from multiyear daily average temperatures.

2. The extreme ambient temperature cycle that is a sine wave with a one-year period which captures the coldest and the hottest of the extreme ambient temperatures. It is used to take into account the possibility of seasons (months) having much higher or lower temperatures than the average ambient conditions based on multiyear averages.

3. The daily temperature cycles, which may be used in areas were daily temperature variation can be 28^oC or more.

Figure 4.1 shows a normal and an extreme annual cycle based on multiyear monthly average temperatures for the construction site of Rialb RCC dam.

The ambient temperature data will also be used in the computation of concrete placement temperature.

Solar radiation. To take into account the increased concrete temperature at the surfaces during construction due to solar radiation, an increase in ambient temperature of 0.5 to 1.0^oC can be incorporated in the thermal analysis (U.S. Army Corps of Engineers (U.S.ACE), 1997).

Concrete properties

The thermal, mechanical and physical properties needed for thermal analysis have already been discussed in Section 2.2.

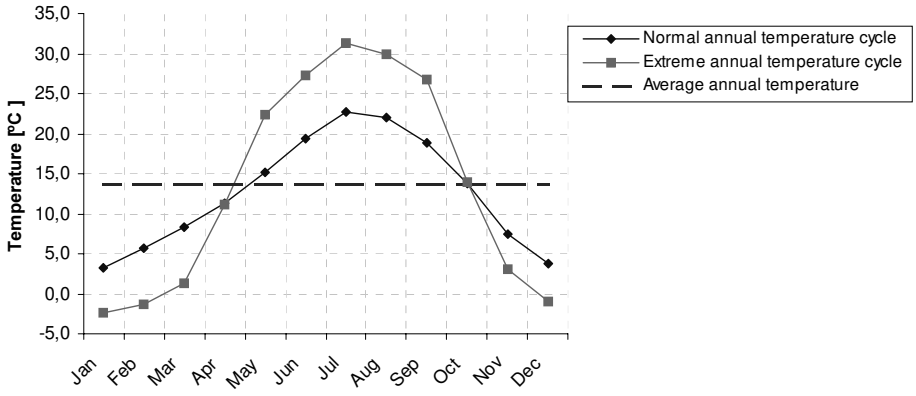

Figure 4.1: Normal and extreme annual temperature cycle.

Construction parameters

Differences in the way a RCC dam is constructed will impact its thermal behavior significantly.

Lift height. Since the heat flow out of a mass is inversely proportional to the square of its least dimension and since the thickness of a lift will be the smallest dimension, it can become an important factor in the thermal behavior. On the other hand, commonly used lift thickness in RCC dams (except for the RCD dams constructed in Japan) only vary between 250 mm and 400 mm.

Lift placement rate. The time between the placement of lifts has an important effect on the thermal performance of the structure due to the insulating effect that a new lift has on the previous lifts. The time between placement of lifts must be included in the thermal analysis. Usually, short time intervals between lifts, *i.e.*, higher placement rates, cause higher temperature in the core of the dam. The longer the interval between placement of lifts, the longer each lift will have to dissipate the heat that have built up within the lift.

Concrete placement temperature. The concrete placement temperature is the most important tool to control the temperature level within the mass of a RCC dam due to the heat of hydration, as well as to control temperature at its surface. In thermal analysis, the placement temperature is the starting point for concrete temperature rise. The concrete placement temperature is mainly influenced by the annual ambient temperature cycle.

Factor	May	Jun	Jul	Aug	Comments
Avg. annual temperature	13.0	13.0	13.0	13.0	Base temperature, measured data
Previous month temperature	12.0	15.4	20.0	22.3	measured data
Added ambient temperature	-0.7	1.6	4.7	6.2	0.67·(Prev. month temp. -avg. annual temp)
Aggretgate subtotal temperature	12.3	14.6	17.7	19.2	Avg. annual temp. + added amb. temp.
Added processing temperature	1.1	1.1	1.1	1.1	Processing and crushing energy
Aggregate stockpile temperature	13.4	15.7	18.8	20.3	
Current ambient temperature	15.4	20.0	22.3	21.5	measured data
Added ambient temperature	1.3	2.9	2.4	0.8	0.67·(Curr. amb. temp. - aggr. stock. temp.)
Added mixer energy	1.1	1.1	1.1	1.1	mixer energy
Placement temperature	15.8	19.7	22.2	22.2	aggr. stock. temp. + added effects

Table 4.1: Placing temperature computation. Temperature [C].

The U.S.ACE established a model which calculates the RCC placing temperature using the average annual temperature modified by rule-of-thumb temperature effects during production (U.S. Army Corps of Engineers (U.S.ACE), 1997). In Table 4.1, the placing temperature is the composite temperature of the aggregate source (assumed to be the average annual temperature), plus the added heat during aggregate production. Stockpile aggregate temperatures are the base temperature, plus the ambient additions and mixer energy additions. Similarly, RCC production temperatures are the stockpile temperature plus ambient additions and mixer energy additions. The ambient temperature additions are calculated as 0.67, an empirical correction factor, times the differential temperature of the aggregates and the air. Figure 4.2 compares the multiyear average monthly temperature of Rialb construction site with the RCC placing temperature.

Construction start date. The time of the year when construction is started has a significant effect on the thermo-mechanical behavior of the dam. Different start dates may cause temperature problems at different locations.

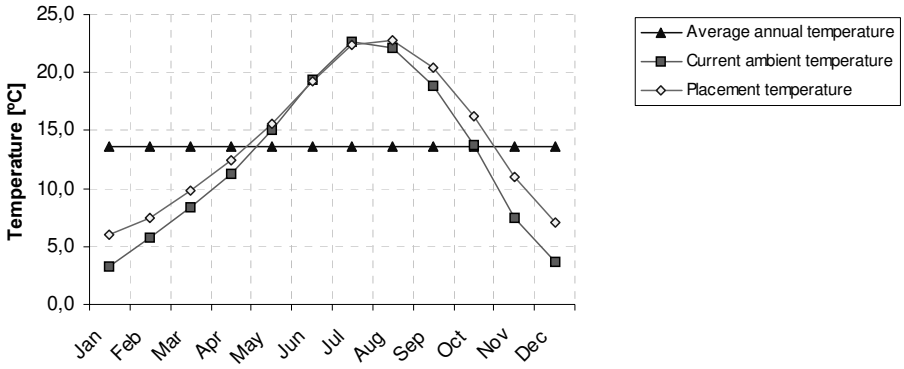

Figure 4.2: RCC placing temperature.

4.5 Mechanical Analysis

As with thermal analysis, there are different methodologies to perform a mechanical analysis of a RCC dam. The less complex method for analysis of cracking is performed based on the computed concrete temperature distributions using simplified procedures to relate thermal changes in volume of the dam structure to estimate cracking potential. The procedures involve approximations and require assumptions regarding conditions of restraint, *i.e.,* the thermally induced strain is computed considering the coefficient of expansion, the temperature difference in concrete causing the strain, and a factor considering the external restraint or internal restraint (U.S. Army Corps of Engineers (U.S.ACE), 1997).

A more accurate form of a mechanical analysis of the structure is to simulate the evolution of stresses in the dam and to evaluate the risk of thermally induced cracking by using a model which takes into account the evolution of the mechanical properties such as strength, modulus of elasticity, and creep, depending on time and on temperature evolution. In the following chapter a thermo-chemo-mechanical model is described, which considers the more relevant features of the behavior of concrete, such as hydration, aging, creep, and damage.

4.6 Models for Thermal-Mechanical Analysis

4.6.1 General Considerations

The analysis of the temperature evolution in RCC dams is a problem which considers a variable domain with each advance in concreting. Therefore, it is essential to use evolutionary models in the simulation, which adapt themselves at each sequence of the computation to the configuration of the dam in this moment, in order to obtain adequate results. An evolutionary model consists of a sequence of n models, each of them reproducing an interval of time in which geometry is considered to be constant. Adequate conditions of compatibility are established between these models, in order to guarantee continuity in time.

Hydration of concrete is not only highly exothermal but also particularly non linear. Within the first 24 hours of the reaction, the properties of the concrete are changing within minutes. As the reaction progresses, changes of the concrete properties become slower. This problem itself requires an adequate choice of time steps for an efficient numerical simulation, *i.e.* smaller time steps have to be used at early ages of the concrete and larger time steps can be used in the long term. Therefore it is stressed that during the construction phase the time steps are chosen based on the age of the last placed lift.

With respect to the dimension of the heat transfer equation the evolutionary models can be classified in 3-D, 2-D, and 1-D models.

4.6.2 3-D Model

A three-dimensional model is the best replication of the geometry of a RCC dam. Theoretically it permits the study of all the phenomena which take place during and after construction of a dam. But due to various factors, which have to be considered in a thermo-mechanical analysis, a three-dimensional simulation often leads to element sizes and time steps too large to reproduce adequately the construction process and the superficial phenomena.

4.6.3 2-D Model

With respect to temperatures fields in RCC dams the two-dimensional transverse models give the same good results as three-dimensional models do, since the variation of temperature in the cross section is predominant and the longitudinal heat flux is almost zero. Despite the simplification,

these models perform the simulation of the evolution of temperature during construction as well as during the service life of a RCC dam with sufficient accuracy. Although the required CPU time of these models is considerable, the decrease of number of elements in comparison to three-dimensional models permits the use of finer meshes which are able to capture the superficial phenomena better and reproduce the construction process more adequately. However, they are not competitive with the one-dimensional models in case of parameter studies.

In case of a stress analysis, a two dimensional transverse model usually gives good analytical results, that can be used to predict cracks that propagate inward from the surface and cracks originating from the foundation. In order to analyze cracks which propagate vertically from the foundation and are oriented perpendicular to the longitudinal axis of the dam two two-dimensional models, a transverse model and a longitudinal model of a horizontal plane, can be used instead of a three-dimensional model (U.S. Army Corps of Engineers (U.S.ACE), 1994). The limitation of the two-dimensional, longitudinal model, is that it is assumed that symmetry exists on either side of the longitudinal plane, which is not the case. The studies made by the U.S.ACE also show that these models have a slower rate of cooling that the transverse models. Therefore it is necessary to calibrate the longitudinal model using the results of the transverse model. This may be done by adjusting the thermal conductivity of different element sets.

4.6.4 1-D Model

Due to the large dimensions, vertical heat flux preponderates in the core of a RCC dam. During construction, heat exchange with the environment takes place almost exclusively at the upper face of the last placed lift. Therefore a one-dimensional model is sufficient to compute the evolution of temperature during the construction phase, especially regarding the maximum reached temperature.

A strip of elements represents the core of the dam. Figure 4.3 shows the model used for the analysis of Rialb RCC dam. The size of the element does not vary over the height of the dam, and the boundary conditions, except for the upper face of the last placed lift, are considered as being adiabatic.

The simplicity of one-dimensional models and their low computational cost permit to simulate a great number of design possibilities. They also allow to use finer meshes than the two-dimensional and three-dimensional models, which reproduce the construction process more accurately. Therefore this type of model is greatly used to perform parameter-studies.

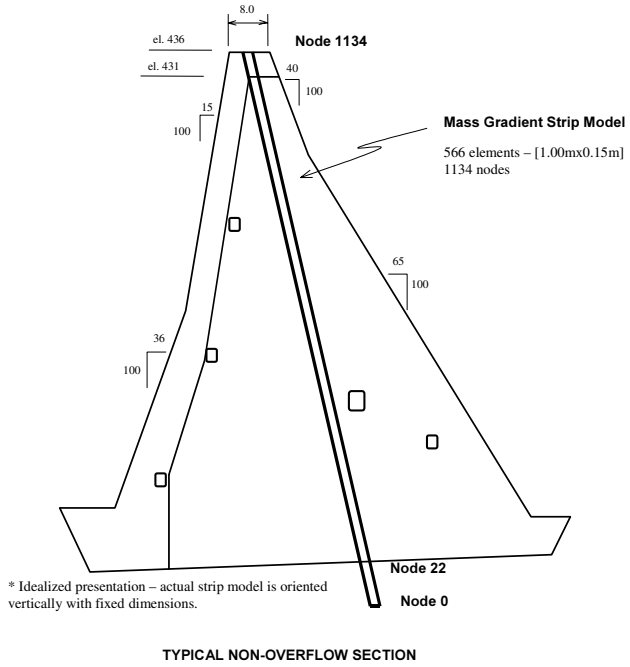

Figure 4.3: 1-D strip model, used for the thermo-mechanical analysis of Rialb RCC dam.

On the other hand, the drawback of usual one-dimensional models is that they do not simulate the horizontal heat flux in the dam body. Consequently, they are not able to simulate the phenomenon of cooling of the core once the dam has been finished. They are not convenient for the analysis of areas close to galleries nor at the crest of the dam, where horizontal heat flux must be considered, when the dam is still under construction.

4.6.5 Summary

Due to the above mentioned, it is easy to understand that the choice between an 3-D, 2-D or 1-D model has a great repercussion in the complexity of the computation. Therefore, it is fundamental to choose the model depending on the type and function of the analysis. Tables 4.2 and 4.3 (taken from (Salete, 1996)) give an overview in the possibilities and applicability of the different models.

Studied phenomen	1-D model	2-D model	3-D model
Temperature rise in areas of great thickness	very good	good	good
Temperature rise in areas of moderate thickness	good	good	good
Temperature rise in areas of minor thickness	bad	acceptable	good
Thermal influence of the galleries	bad	good	good
Evolution of temperature at the surface	very good	good	good

Table 4.2: Quality of adjustment of the different models.

Type of analisys	RCC dams
Feasibilty studies	1-D
Maximum temperature calculation during construction	1-D/2-D
Scheduling of concrete placement preconstruction phase	1-D
Analisys of thermal gradients	1-D/2-D
Scheduling of concrete placement construction phase	1-D fine mesh
Analisys of thermally induced stresses	2-D/3-D
Analisys of thermally induced cracking	3-D

Table 4.3: Recommended models for the different types of analisys.

Chapter 5

Thermo-Chemo-Mechanical Model by Cervera *et al.* (1999)

5.1 Thermo-Mechanical Problem

5.1.1 Thermo-mechanical Interactions

The hardening process of concrete is divided into different subproblems depending on each other, such as:

- chemical problem,
- thermal problem and
- mechanical problem.

The chemical problem (problem of hydration and aging) is represented by only one variable such as the hydration degree of the concrete which describes the development of the microstructure of the material. It shows the complex phenomenon of the hydration and hardening of the cement and controls the quantity and velocity of the hydration heat and the development of the material mechanical properties.

The thermal problem consists on the evaluation of the thermal history of the concrete. This evaluation can be done by using the equation of energy, which is produced for the volume of the material. The fundamental variable of this problem is the temperature. The method used to study this problem is framed into the phenomenological theory, which means in this context that it is based on a macroscopic approach.

Finally, for the mechanical problem the conditions of equilibrium must be satisfied by the stresses developed during the studied process. The method to study this problem is also framed into the phenomenological theory.

The coupling between these three problems can be sufficiently described with four interaction. They are visualized with the help of the scheme given

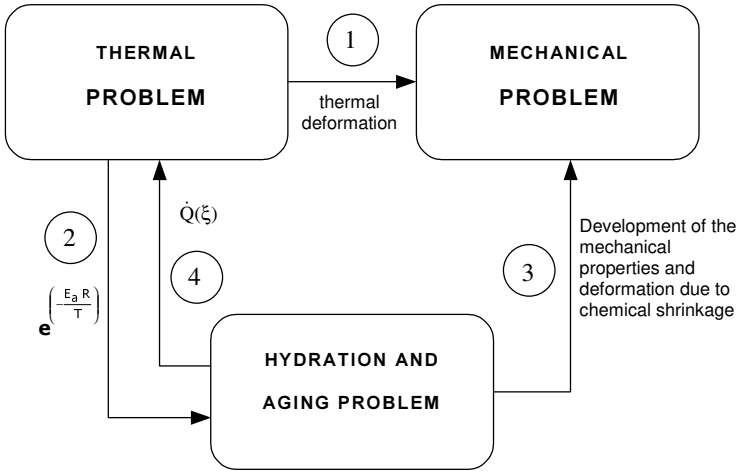

Figure 5.1: Thermomechanical interactions for concrete at early ages.

in Figure 5.1.

Interaction 1 (thermal problem $\longrightarrow$ mechanical problem) refers to the thermal deformations and consequently to the thermally induced stresses within the constitutive model which depend on the temperature.

Interaction 2 (thermal problem $\longrightarrow$ chemical problem) conditions the microstructural transformation of the concrete. Therefore all the microscopic phenomena which are involved in the process of hydration and aging, together with other variables are related to the temperature at which they develop.

Interaction 3 (chemical problem $\longrightarrow$ mechanical problem) refers to the development of the thermal and mechanical properties of the concrete during the process of hydration. It also generates volumetric deformations of the concrete due to hydration (chemical shrinkage).

Interaction 4 (chemical problem $\longrightarrow$ thermal problem) governs the energy changes derived from the phenomenon of hydration of the cement. This heat release modifies the local thermal history of the concrete.

5.1.2 The Governing Equations

The local system of partial differential equations governing the coupled thermo-mechanical problem is defined by the momentum and energy balance equations. They can be written as:

$$\begin{cases} C\dot{T} - \dot{Q}(\xi) = R_{ext} - \boldsymbol{\nabla} \cdot \mathbf{Q} \\ \mathbf{0} = \boldsymbol{\nabla} \cdot \boldsymbol{\sigma} + \mathbf{b} \end{cases} \tag{5.1}$$

where C is the heat capacity, T the temperature, R_{ext} represents the heat production of the external volume heat sources and $\mathbf{Q}$ is the heat

flux. In the momentum equation $\mathbf{b}$ describes the body forces, $\boldsymbol{\nabla} \cdot (\cdot)$ is the divergence operator and $\boldsymbol{\sigma}$ is the stress tensor.

5.1.3 Time Integration of the Coupled Model

The numerical simulation of the coupled thermo-mechanical problem involves the transformation of a system of differential governing equations into a sequence of discrete algebraic problems by means of a Galerkin finite element projection and a defined time marching scheme.

Time marching schemes for the advancement of the main variables (displacements and temperatures) can be grouped in two categories: simultaneous time-stepping algorithms and staggered time-stepping algorithms.

Simultaneous time-stepping algorithms solve both, the mechanical and the thermal equilibrium equations together, thus advancing of the displacements and temperatures, simultaneously. It leads to large and unsymmetrical systems of equations and usually it is expensive to solve.

Staggered time-stepping algorithms are based on the use of an operator split, applied to the coupled system of differential equations, and a product formula algorithm, which leads to a scheme in which each on of the subproblems defined by the partitions is solved sequentially, within the framework of the classical fractional step method. This leads to the partition of the original coupled problem into smaller and typically symmetric subproblems. In COMET this staggered scheme has been preferred.

In the classic isothermal split the coupled system of equations is partitioned into a mechanical phase at constant temperature, followed by a thermal phase at fixed configuration. In both phases the internal variables Γ_n, such as the damage tensile/compressive thresholds (r^+,r^-), respecting the micro prestress (μ), hydration degree (ξ) and aging degree (κ) are updated.

The stress development during the early ages of concrete is basically activated by the variation of temperature. Therefore it is advantageous to consider a scheme where the thermal phase of the operator split is performed before the mechanical phase. The mechanical problem is then solved by using the updated field temperature, T_{n+1}. Table 5.1 represents the two phases at each time step. The time integration of a quasi-static problem consists of finding the amounts of the displacements u_{n+1} and the temperatures T_{n+1} from a known solution of u_n and T_n. In COMET a Backward Euler scheme is used.

Thermal Problem
u_n, T_n and Γ_n
$\downarrow$
u_n, T_{n+1} and $\tilde{\Gamma}_{n+1}$
Mechanical Problem
u_n, T_{n+1} and $\tilde{\Gamma}_{n+1}$
$\downarrow$
u_{n+1} and Γ_{n+1}
u_{n+1}, T_{n+1} and Γ_{n+1}

Table 5.1: Scheme for advancing in time.

5.2 The Constitutive Model

The following section presents the thermo-chemo-mechanical model developed by Cervera *et al.* (1999) which considers many of the relevant features of the hydration, aging and mechanical behavior of concrete, in a format suitable for its implementation in the general framework of the Finite Element Method.

5.2.1 Hydration and Aging Model

Hydration model

From the first and second principles of thermodynamics the thermal field equation can be written, as

$$C\dot{T} - \dot{Q}(\xi) = R_{ext} + k_T \nabla \cdot (\nabla T) \tag{5.2}$$

where T is the temperature, C the heat capacity per unit volume, $\dot{Q}$ the velocity of liberated heat per unit volume, R_{ext} is the heat production of the external volume heat sources and k_T is the thermal conductivity. Note that the term due to the hydration heat, $\dot{Q}$, actually acts as a nonlinear internal heat source. Besides the Fourier's Law ($\mathbf{Q} = -k_T \nabla T$) has been used (see Eq.5.2).

The thermo-chemical model must provide the determination of this term depending on the hydration heat. The thermo-chemical model regards the evolution of the chemical reaction of concrete hydration and the heat generated during the process. It is based on the Theory of Reactive Porous Media, within a consistent thermodynamic framework. The assumption of a closed chemical system allows a local description of the internal variables.

For practical purposes, it is convenient to write the model in terms of a normalized variable called hydration degree, ξ. Most authors identify the rate of liberated heat with the rate of the hydration. In this case, the

hydration degree can be also defined $\xi = Q/\bar{Q}_\infty$ with $\xi_\infty < 1$, where $\bar{Q}_\infty$ is the final amount of liberated heat in ideal conditions. The final degree of hydration ξ_∞ can be estimated with the equation:

$$\xi_\infty = \frac{1.031 w/c}{0194 + w/c} \tag{5.3}$$

This is equivalent to assume a linear dependency of the form

$$Q(\xi) = Q_\xi \xi \tag{5.4}$$

where Q_ξ is the latent heat, here assumed a constant material property.

By assuming that the hydration reaction is thermoactivated, development of hydration degree can be defined with an Arrhenius type equation such as

$$\dot{\xi} = \widetilde{A}_\xi(\xi) \exp\left(-\frac{E_a}{RT}\right) \geq 0 \tag{5.5}$$

where E_a is the activation energy of the reaction, R is the constant for ideal gases, see Ulm and Coussy (1996). The ratio E_a/R can be experimentally determined, and it ranges from 3000 to 8000 K for concrete. The function $\widetilde{A}_\xi(\xi)$ represents the normalized affinity that completely characterizes the macroscopic hydration kinetics for a given concrete mixture. This function can also be obtained experimentally from an adiabatic calorimetric test. In this model the following expression with the material constants, such as k_ξ, $A_{\xi 0}$, $\eta_{\xi 0}$ and $\overline{\eta}$, is proposed:

$$\widetilde{A}_\xi(\xi) = \frac{k_\xi}{\eta_{\xi 0}} \left(\frac{A_{\xi 0}}{k_\xi \xi_\infty} + \xi\right) (\xi_\infty - \xi) \exp\left(-\overline{\eta}\frac{\xi}{\xi_\infty}\right) \tag{5.6}$$

Aging Model

The change in the relative proportions and physical properties of the basic constituents of concrete during the chemical reaction of hydration is a phenomenon known as aging.

During the last decades, many aging models have been proposed in which the mechanical properties of young concrete were expressed in terms of the hydration degree, or alternatively, of the maturity. The basic assumption for these models is that concretes of the same mix at the same hydration degree have the same strength independently of the hydration kinetics occurred to reach that hydration degree.

However, there is experimental evidence that the evolution of the concrete strength depends not only on the degree of hydration, but also on the kinetics of the hydration reaction. In view of this, it is concluded that

concrete strength cannot be related directly to the hydration degree, and therefore, the mechanical properties cannot be obtained without the consideration of the hydration kinetics.

A realistic aging model must be established in which the mechanical properties act as internal-like variables, and their evolution laws must be formulated in terms of, at least, hydration degree and temperature.

The aging model regards the evolution of the compressive and tensile uniaxial strengths and the uniaxial elastic modulus during the hydration process of the concrete, These are the basic parameters used in the mechanical damage model. For simplicity, Poisson's ratio is assumed to remain constant. The effect of the curing temperature on the evolution of the compressive strength makes it necessary to relate this evolution to the hydration kinetics. Therefore an aging internal variable, κ, is introduced, so that the compressive strength, f^- can be written as

$$f^-(\kappa) = \kappa\, f^-_\infty \qquad \kappa \geq 0 \tag{5.7}$$

where f^-_∞ is the final compressive strength. Note that κ can be considered a normalized strength variable. Thus, it will be called here *aging degree*.

The evolution of the aging degree must be related to the hydration kinetics and the temperature. The following equation clearly expresses the dependency of the aging variable both on the hydration degree and on temperature:

$$\dot{\kappa} = (A_f \xi + B_f) \left(\frac{T_T - T}{T_T - T_{ref}} \right)^{n_T} \dot{\xi} \tag{5.8}$$

where T_{ref} is the reference temperature for the determination of f^-_∞, T_T represents the maximum temperature at which hardening of concrete may occur and n_T is a material property.

The final tensile strength and the final elastic modulus are usually considered to be related to the final compressive strength and therefore to the aging degree, such as

$$f^+(\kappa) = \kappa^{2/3}\, f^+_\infty \tag{5.9}$$

and

$$E(\kappa) = \kappa^{1/2} E_\infty \tag{5.10}$$

where f^+_∞ and E_∞ are the final values at the end of hydration.

5.2.2 Damage and Creep

The mechanical behavior of concrete is complex and highly nonlinear. In order to describe the mechanical aspects of concrete the short and long term mechanical behavior is modelled via a viscoelastic damage model which accounts for the aging effects.

The basic idea is to use a viscoelastic aging model, able to reproduce the creep and relaxation phenomena typical of long term behavior of concrete. This must be coupled to a damage model, also considering the relevant thermal and chemical effects. Long term effects are included by incorporating a creep model inspired in the Microprestress-Solidification Theory.

The short term model is based on the framework of the Continuum Damage Mechanics Theory. It makes use of an isotropic damage model, with only two scalar internal variables to monitor the local damage under tension and compression, respectively. It takes the temperature effects and the phenomenon of aging into account.

Microprestress-Solidification Theory

The rheological model which is used to represent the long term mechanical behavior of concrete consists of a viscoelastic chain, with the elastic moduli, E^i, and the dashpot viscosities, η^i, of the $i = 1, ..., N$ Maxwell elements as material parameters. It is also helpful to consider the elastic moduli, E^i, and the relaxation times of the dashpots, defined as $\tau^i = \eta^i / E^i$, as an alternative characterization of the chain.

Figure 5.2 shows a schematic representation of the rheological model used for long term behavior, in the form of a Maxwell chain. In the framework of aging models the general case of such a rheological model would consist of independently varying elastic moduli and dashpot viscosities. However, it is usual to restrict the model to the consideration of proportional varying elastic moduli and constant relaxation times.

In the following it will be assumed that during the aging process all the elastic moduli vary proportionally to the aging function defined by the aging model, $E^i(\kappa) = \lambda_E(\kappa)\, E^i_\infty$ (where E^i_∞ are values at the end of the hydration process, and $E_\infty = \sum_{i=1}^{N} E^i_\infty$), and that the relaxation times, τ^i, remain constant. It was shown in Carol and Bazant (1993) that this is equivalent to the model arising from Solidification Theory, Bažant and Prasannan (1989), with a non-aging Maxwell chain for the basic constituent.

The total stress sustained by the Maxwell chain is evaluated as

$$\boldsymbol{\sigma} = \sum_{i=1}^{N} \boldsymbol{\sigma}^i \tag{5.11}$$

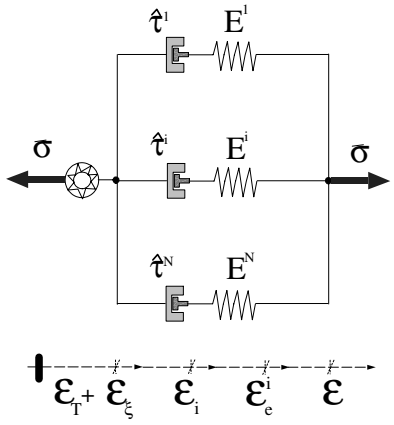

Figure 5.2: Rheological model for long term behavior.

Choosing the stress in each Maxwell element of the chain, $\boldsymbol{\sigma}^i$, as internal variables, it was shown in Carol and Bazant (1993) that the first order differential equations governing the evolution of these variables are

$$\dot{\boldsymbol{\sigma}}^i + \frac{\sigma^i}{\tau^i} = \lambda_E(\kappa) E^i_\infty \overline{\mathbf{D}} \dot{\boldsymbol{\varepsilon}} \quad \text{for} \quad i = 1, ..., N \tag{5.12}$$

where tensor entities are used as the multidimensional counterparts of the scalar ones used for uniaxial models; ε is the total strain tensor and the non-dimensional tensor $\overline{\mathbf{D}} = (1/E)\mathbf{D}$ has been used. where $\mathbf{D}$ is the (fourth order) linear–elastic constitutive tensor, which gives the information about the elastic behavior of the material.

The proposed model cannot be the final solution of the long term aging because the duration of creep for a fixed load decreases significantly with an increasing age at loading even after many years, while the hydration degree essentially stops before one year of age. This experimental evidence was considered in the Solidification Theory, Bažant and Prasannan (1989), by including a flow element with a time dependent viscosity. A physical model is formulated to obtain the viscosity of the flow dashpot as a function of the tensile micro-prestress carried by the bonds and bridges crossing the gel pores in the hardened cement gel. The long term creep is assumed to originate from viscous shear slips between the opposite walls of micropores in which the bonds that transmit the micro-prestress break and reform. Let σ_μ be the value of the micro-prestress and η_μ be the value of the viscosity of the corresponding flow term.

With $\sigma_{\mu 0}$ and $\eta_{\mu 0}$ as initial values, it can be assumed that the viscosity is inversely proportional to the micro-prestress, so that $\sigma_\mu/\sigma_{\mu 0} = \eta_{\mu 0}/\eta_\mu = \mu$ where μ is a variable that can be regarded as the normalized value of the micro-prestress.

If humidity effects are not considered (sealed specimens, basic creep), the evolution of the normalized micro-prestress can be explicitly determined as: $\mu(t) = 1/(1 + c_{\mu 0}\, t)$, where $c_{\mu 0}$ is a material property. The relaxation time of the flow term as $\tau_\mu = (\tau_{\mu 0}\, E_\infty)/(\mu\, E)$, where $\tau_{\mu 0} = \eta_{\mu 0}/E_\infty$ is a material property. Note that as time increases, the micro-prestress decreases, and so the viscosity of the flow term increases. Eventually, the micro-prestress will vanish, the viscosity will tend to infinity and the flow term will become inactive.

Now, Eq. (5.12) has to be modified to include the effect of the nonlinear flow term:

$$\dot{\boldsymbol{\sigma}}^i + \left(\frac{1}{\tau^i} + \frac{1}{\tau_\mu}\right)\boldsymbol{\sigma}^i = E^i(\kappa)\overline{\mathbf{D}}\dot{\boldsymbol{\varepsilon}} \quad \text{for} \quad i = 1, ..., N \tag{5.13}$$

Note that the effect of the flow term is completely defined with two additional material properties: $\tau_{\mu 0}$ and $c_{\mu 0}$. The first one defines the initial value of the viscosity, and the second one governs its rate of evolution.

Instead of the stress, $\boldsymbol{\sigma}^i$, the viscous strains in each Maxwell element, $\boldsymbol{\varepsilon}^i$ can be selected as internal variables alternatively.

$$\boldsymbol{\sigma}^i = E^i(\kappa)\bar{\mathbf{D}} : (\boldsymbol{\varepsilon} - \boldsymbol{\varepsilon}^i) \tag{5.14}$$

Substitution of Eq. (5.14) into Eq. (5.13) leads to the obtention of the evolution law for the viscous strains

$$\boldsymbol{\varepsilon}^i = \left(\frac{1}{\tau^i} + \frac{1}{\tau_\mu} + \frac{1}{\tau_a}\right)(\boldsymbol{\varepsilon} - \boldsymbol{\varepsilon}^i) = \frac{1}{\hat{\tau}^i}(\boldsymbol{\varepsilon} - \boldsymbol{\varepsilon}^i) \qquad \text{for} \quad i = 1, ..., N \tag{5.15}$$

with $\tau_a(\kappa) = E/\dot{E}$ representing the aging effect on the elastic modulus. Note that even if τ^i and τ_μ are sufficiently large, there would be some viscous straining as long as the aging progresses and the elastic modulus varies ($\dot{\lambda}_E \neq 0$). As time increases, the rate of hydration decreases, and so the viscosity due to aging increases. Eventually, $\tau_a(t = \infty) = \infty$ and the model would revert to a standard Maxwell viscoelastic arrangement.

Resuming the total relaxation time of the Maxwell chain depend on the summary of the inverse relaxation time of the dashpot, on the flow term, due to the micro-prestresses, and on the inverse relaxation time respecting the aging effect on the Young modulus, such as

$$\frac{1}{\hat{\tau}^i} = \left(\frac{1}{\tau^i} + \frac{1}{\tau_\mu} + \frac{1}{\tau_a}\right) \qquad \text{for} \quad i = 1, ..., N \tag{5.16}$$

Aging Viscoelasticity and Damage

The Continuum Damage Theory was firstly introduced by Kachanov (1958) in the context of creep–related problems, but it has afterwards been accepted as a valid alternative to deal with complex material behavior. It is

nowadays used for a variety of materials as metals, ceramics, rock and concrete, and within a wide range of applications (creep, fatigue, progressive failure, etc.). The reason for its popularity is as much the intrinsic simplicity and versatility of the approach, as well as its consistency, based on the theory of thermodynamics of irreversible processes.

Finally the coupling of the viscoelastic model with a aging damage model is described, as well as the relevant thermal and chemical couplings. The basic hypothesis is that the stress sustained by the Maxwell chain is the effective (undamaged) stress, instead of the total stress. This idea is based on the Continuum Damage Mechanics Theory (CDMT) concept: the effective stress acts on the effective (undamaged) solid concrete, while the total stress acts on the whole (damaged) solid.

The effective stresses and the elastic strains for one element of the Maxwell chain can be defined as:

$$\overline{\sigma}^i \left(\varepsilon_e^i, \kappa\right) = E^i(\kappa)\, \overline{\mathbf{D}} : \boldsymbol{\varepsilon}_e^i \tag{5.17}$$

with

$$\boldsymbol{\varepsilon}_e^i(\boldsymbol{\varepsilon}, \boldsymbol{\varepsilon}^i, T, \xi) = \boldsymbol{\varepsilon} - \boldsymbol{\varepsilon}_T - \boldsymbol{\varepsilon}_\xi - \boldsymbol{\varepsilon}^i \tag{5.18}$$

where T is the temperature and ξ the hydration degree and (:) denotes the tensor product contracted on two indices. Note that the thermal, $\varepsilon_T = \alpha_T \left(T - T_{ref}\right) \mathbf{1}$, and the chemical, $\varepsilon_\xi = \alpha_\xi \xi \mathbf{1}$, volumetric strains affect all the elements in the same way, but the viscous strain tensor, ε^i, is different for each Maxwell element.

The actual defined reference temperature T_{ref} in the constitutive model is equal to the temperature reached at the end of the setting phase (when $\xi = \xi_{set}$), so that the material begins the behavior of a solid, and the process of thermally induced stresses starts. Values $\xi_{set} = 0.1$ to 0.4 have been proposed in the literature, depending on the type of cement and the water/cement ratio.

Inspired by Faria *et al.* (1998) the stress split for each element, as

$$\bar{\boldsymbol{\sigma}}^{i+} = \sum_{j=1}^{3} < \overline{\sigma}_j^i > \mathbf{p}_j^i \otimes \mathbf{p}_j^i \qquad \text{and} \qquad \bar{\boldsymbol{\sigma}}^{i-} = \bar{\boldsymbol{\sigma}}^i - \bar{\boldsymbol{\sigma}}^{i+} \tag{5.19}$$

where $\overline{\overline{\sigma}}_j^i$ denotes the *j–th* principal stress value from tensor $\overline{\overline{\sigma}}^i$, $\mathbf{p}_j^i$ represents the unit vector associated with its respective principal direction and the symbol $\otimes$ denotes the tensor product. The symbols $< . >$ are the Macaulay brackets ($< x >= x,$ if $x \geq 0, < x >= 0,$ if $x < 0$).

The stresses are obtained with the following constitutive equation which relates the stresses with the deformation for each Maxwell element,

$$\boldsymbol{\sigma} \;=\; (1 - d^+) \sum_{i=1}^{N} \overline{\boldsymbol{\sigma}}^{i+} + (1 - d^-) \sum_{i=1}^{N} \overline{\boldsymbol{\sigma}}^{i-}$$

$$= \quad (1 - d^+)\overline{\sigma}^+ + (1 - d^-)\overline{\boldsymbol{\sigma}}^- \tag{5.20}$$

where two internal-like variables, d^+ and d^-, the damage indices under tension and compression, are introduced, respectively. The behavior through time of d^+ and d^- are described by constitutive evolution equations.

Chapter 6

Thermo-Mechanical Analysis of Rialb RCC Dam

6.1 Rialb Dam

The Rialb RCC dam is situated in the province of Lleida (Spain), between the regions of La Noguera and L'Alt Urgell. The reservoir is on the river Segre which is a tributary of the river Ebro and the closure has been constructed 4 km from Ponts. The zone has Mediterranean climate. Its annual mean climate values are as follows: temperature, 12.8^oC (ranging from 2.8^oC in winter to 23.3^oC in summer), relative humidity, 67% and annual rainfall 304 mm.

The purpose of the Rialb reservoir is to control the river Segre in order to meet the water demands of the irrigated areas Canal d'Urgel, Canal Segarra-Garrigues, Garrigues Altas and Garrigues Bajas. In addition to this, the reservoir helps in the water supply requirements of 200,000 inhabitants in 80 centres of population, it provides an ecological flow of 3.50 m^3/s and it controls any extraordinary floods. There is also the possibility of building a transformer station at the foot of the dam.

6.1.1 Geometry

The dam is a straight RCC gravity structure 595 m long and 101 m high. The total concrete volume of the dam is 1,200,000 m^3 of which 1,050,000 m^3 are RCC (see Table 6.1). This makes it the largest volume RCC dam in Europe. The slope of the upstream face is $H/V = 0.35$ from the foundation until elevation 386.0 m and from there until the crest (elevation 436.0 m) $H/V = 0.15$. The slope of the downstream face is $H/V = 0.65$ from the foundation until elevation 416.0 m and from there to the crest $H/V = 0.40$. This shape of cross section is chosen because of seismic calculations. The

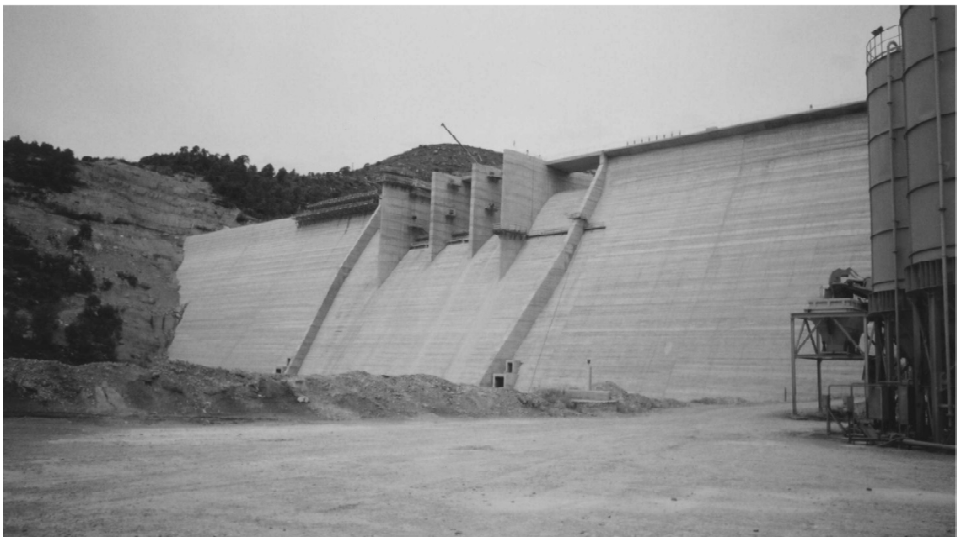

Figure 6.1: Rialb RCC dam.

dam is located in an area where seismic activity is expected.

A 82.2 m long spillway section is incorporated in the dam at its right extremity. The surface spillway which consist of three 12 m central openings with gates of Taintor type (12 x 7.40 m) and two 16.50 m fixed lip openings is built on top of the dam.

The dam is divided in 16 blocks, separated by vertical joints, placed in a continuous line from the crest down to the point where the RCC reaches the conventional concrete of the foundation. The distance of the contraction joints is 28.75 m next to the spillway section and 40 m in the rest of the dam (Figure 6.2).

Type	RCC gravity dam
Crest level	436 m
Crest length	595 m
Heigth above foundation	101 m
Volume of concrete	1,200,000 m^3
Volume of RCC	1,050,000 m^3
Lift height	30 cm
Foundation gradient	7%
Project start	1/1993
Project finish	2/2000
Basin surface area	3,320 km^2
Dam surface	1,505 ha
Reservoir capacity	402,000,000 m^3

Table 6.1: Characteristics of the Rialb dam.

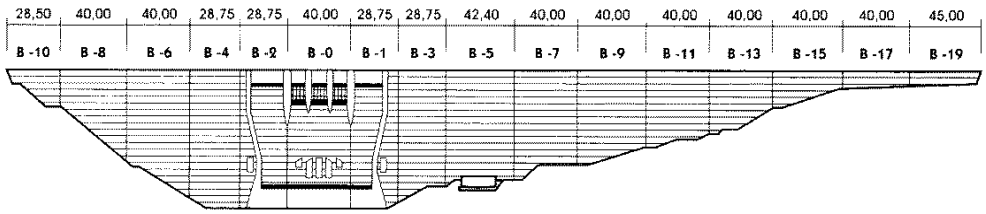

Figure 6.2: Distance of the contraction joints.

	HC-1	HC-2
S_{max} $[mm]$	70	100
Cement $[kg/m^3]$	70	65
Pozzolan $[kg/m^3]$	130	130
$c+f$ $[kg/m^3]$	200	195
water $[kg/m^3]$	90	80
$w/(c+f)$	0.45	0.41

Table 6.2: RCC mixes used at the Rialb dam.

6.1.2 Material Properties

Five types of concrete were used in the dam (Figure 6.3). Due to the current trend of construction consisting of not placing any impermeable membrane at the upstream face, the body of the dam comprise the two types of RCC, HC-1 and HC-2 (see Table 6.2). The HC-1 concrete which contains aggregates of five sizes (70 mm maximum) and a paste content of 200 kg/m^3, providing thus high impermeability, is placed in the up-stream section. For the HC-2 concrete, which is building the main body, six sizes of aggregates and a past content of 195 kg/m^3 are used. The facings except for the spillway section are made of slip-formed elements. To fulfill the demands of erosion resistance due to hydraulic activations, the spillway section was build using a conventional placed concrete with a cementitious content of 280 kg/m^3 (205 kg/m^3 of cement, 75 kg/m^3 of fly ash) and addition of metallic fibers. A 1 m thick layer of conventional vibrated concrete, with aggregates of four different sizes, was spread over the whole foundation surface, serving as an interface between the foundation and the dam.

Table 6.3 summarizes the relevant material properties for the RCC, the conventional concrete of the foundation and the foundation rock. The rest of the material properties of the HC-1 (see Table 6.4) necessary to perform the numerical simulations have been obtained by calibration of the model parameter to match experimental data obtained from laboratory tests. The comparison between the model performance and the available experimental results is shown in Figure 6.4, where the asterisks represent the experimental

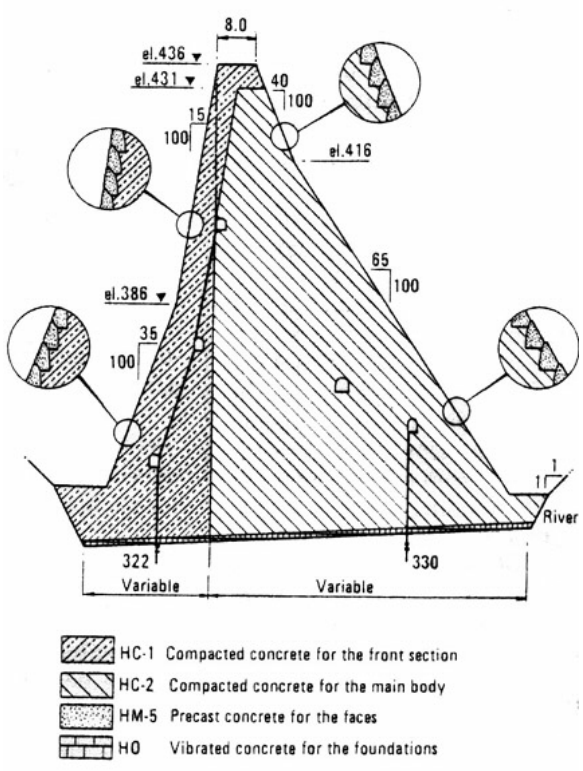

Figure 6.3: Section of Rialb dam.

values and the solid lines represent the predictions by the model. Figure 6.4(a) shows the evolution of the temperature obtained in adiabatic tests, and Figure 6.4(b) shows the evolution of compressive strength obtained in isothermal tests. Note that good agreement is obtained between the model predictions and the experimental results.

It should be mentioned that the experimental data of the adiabatic temperature rise only represent the first five days, although the chemical reaction and so the generation of heat takes place over a much longer period of time. It is assumed that, in case of ideal adiabatic conditions the final temperature rise would take a value of 19.79^oC (see Figure 6.5).

Likewise, the final value of strength does not correspond to the value reached after 180 days, since for a concrete, containing 65% of fly ash of cementitious material the final strength is reached later. The value of final strength has been taken as 42 MPa for the HC-1, *i.e.*, assuming an increase of 15% with respect to the value obtained after 180 days. With regard to the influence of the conditions of curing, $\eta_T = 0$ was taken, due to the lack of sufficient information to estimate the effect of temperature in the final strength.

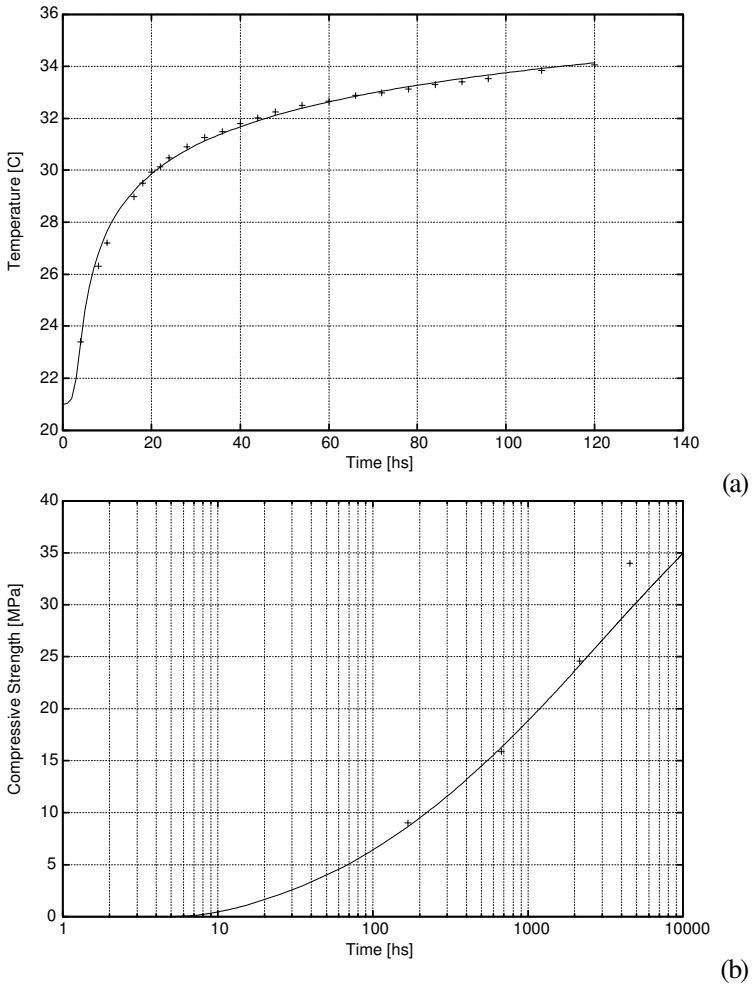

Figure 6.4: (a) Evolution of temperature under adiabatic conditions. (b) Evolution of compressive strength under isothermic conditions.

Properties	HC-1	HC-2	H0	Foundation
$w/(c+f)$ $[10^3 kg/m^3$	0.45	0.41	1.00	–
ρ $[10^3 kg/m^3]$	2.50	2.50	2.44	2.70
C $[10^6 J/m^{3o}C]$	2.44	2.44	2.44	2.37
k_T $[10^3 J/mhs^oC]$	7.10	7.10	6.81	7.74
α_T $[10^{-6}]$	7.80	7.80	8.00	–
Q_ξ $[10^7 J/m^3]$	7.00	7.00	7.79	–
f_∞^- $[MPa]$	42.00	40.00	30.00	50.00
f_∞^+ $[MPa]$	4.20	4.00	3.00	5.00
E_∞ $[GPa]$	23.00	23.00	31.00	40.00

Table 6.3: Material properties for Rialb dam.

Properties	HC-1
w/c	0.41
ξ_∞	0.70
$k_\xi/\eta_{\xi 0}$ $[10^8\ 1/hs]$	0.70
η	10.50
$A_{\xi 0}/k_\xi$ $[10^{-4}]$	1.00
E_a/R $[10^{3o}K]$	5.00
Q_ξ $[10^7 J/m^3]$	7.00
ξ_{set}	0.30
f_∞^- $[MPa]$	42.0
f_∞^+ $[MPa]$	4.20
T_T $[^oC]$	100.0
T_{ref} $[^oC]$	21.0
n_T	0.00

Table 6.4: Material properties for the numerical simulation.

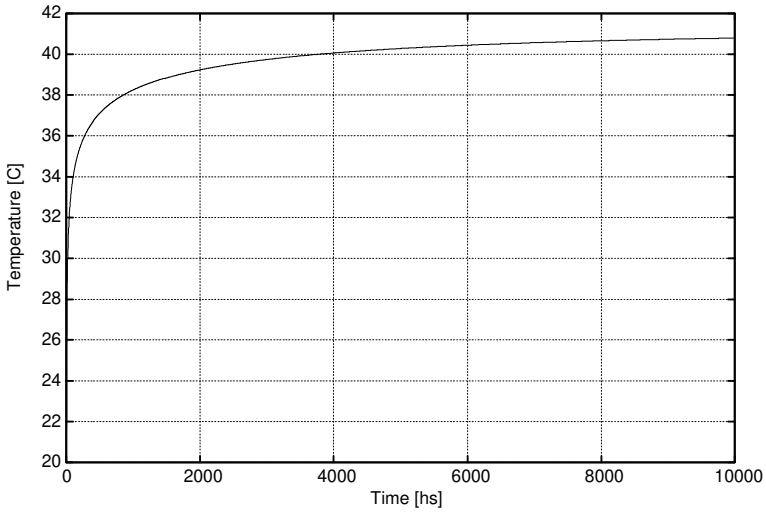

Figure 6.5: Adiabatic temperature rise in the long term.

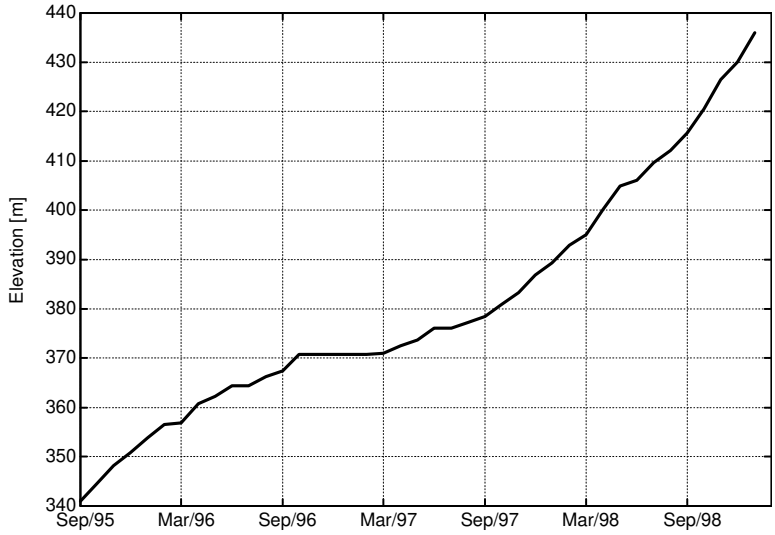

Figure 6.6: Construction schedule of block 1.

6.1.3 Construction Process

Excavation and earthwork for the Rialb dam started in 1993. After completing foundation preparation in summer 1995, the construction of the dam body began with concreting of the foundation. RCC placing started in September 1995 and was finished in December 1998 in case of the Block 1, and in April 1999 for the whole dam. The placement of RCC was interrupted from October 1996 until March 1997, because sufficient fly ash to produce the concrete was not available during this period. To provide water during the agricultural season, part of the reservoir was filled during the summer of 1999. After completing final works the dam started full operation in February 2000.

Figure 6.6 shows the construction process of the Block 1. It can be observed the average monthly placing speed as well as all the interruptions of the construction.

The dam was built with 30 *cm* thick lifts. In order to achieve high bond at the lift joints, 6 to 10 lifts are placed consecutively. This means that the next lift is placed 6 to 8 hours after the previous lift. To avoid high temperature rises in the core, there was an interval of 10 to 20 days between each group of lifts. Placing the RCC in this manner produced less horizontal cold joints and allowed heat dissipation due to the convection phenomena with the environment.

6.2 Reference Case

In this section, results from the thermo-mechanical analyses of Rialb dam are presented. The simulation includes the real construction process as well as the long term behavior of the dam. To simulate the behavior of the dam after its construction a modified 1-D strip model is used. The obtained results are compared with the temperatures measured in the dam during the time of construction.

6.2.1 Numerical Model

Since the analysis was performed some time after the construction of the dam, actual conditions, such as ambient temperatures, placing schedules, and material properties were used in the model. The numerical model used for the thermo-mechanical analysis consists of a modified 1-D strip model. The mesh represents the core of the dam (from elevation 344.60 m to elevation 428.00 m), plus the foundation (from elevation 344.60 m to elevation 337.60 m), and some surrounding foundation rock (down to elevation 328.60 m).

The model permits to simulate the evolutionary construction process and the behavior of the dam during its service life. The time step sizes used in the analysis during construction of the dam are either of 3 h or of 4 h, so that once a lift has been activated, a certain number of time steps pass before the next lift, which is placed above, is activated. The 3 h and 4 h time steps are chosen based on the construction process, and on the fact that they satisfied the maximum time interval required to compute early heat gain in the concrete. When parts of the dam start to cool down, so called slidelines or convection lines, which are placed at both sides of the strip, are activated in the model. Once a slide line has been activated, the temperature of the corresponding elements decrease due to horizontal heat flux (see Figure 6.7).

Every lift is dicretized using 2 four-node elements, thus resulting in 556 elements in the dam body. The total number of elements in the mesh is 612 including the foundation and the elements used to simulate the cooling.

6.2.2 Thermometers Installed in the Dam Body

A series of thermometers are installed in block 1, whose data are used to verify the numerical model and the assumptions made for the model. The thermometers, which have an accuracy of 0.1^oC are installed at different elevations. Collection and storage of the data is executed automatically. Figure 6.8 shows a plan with the position of the different thermometers.

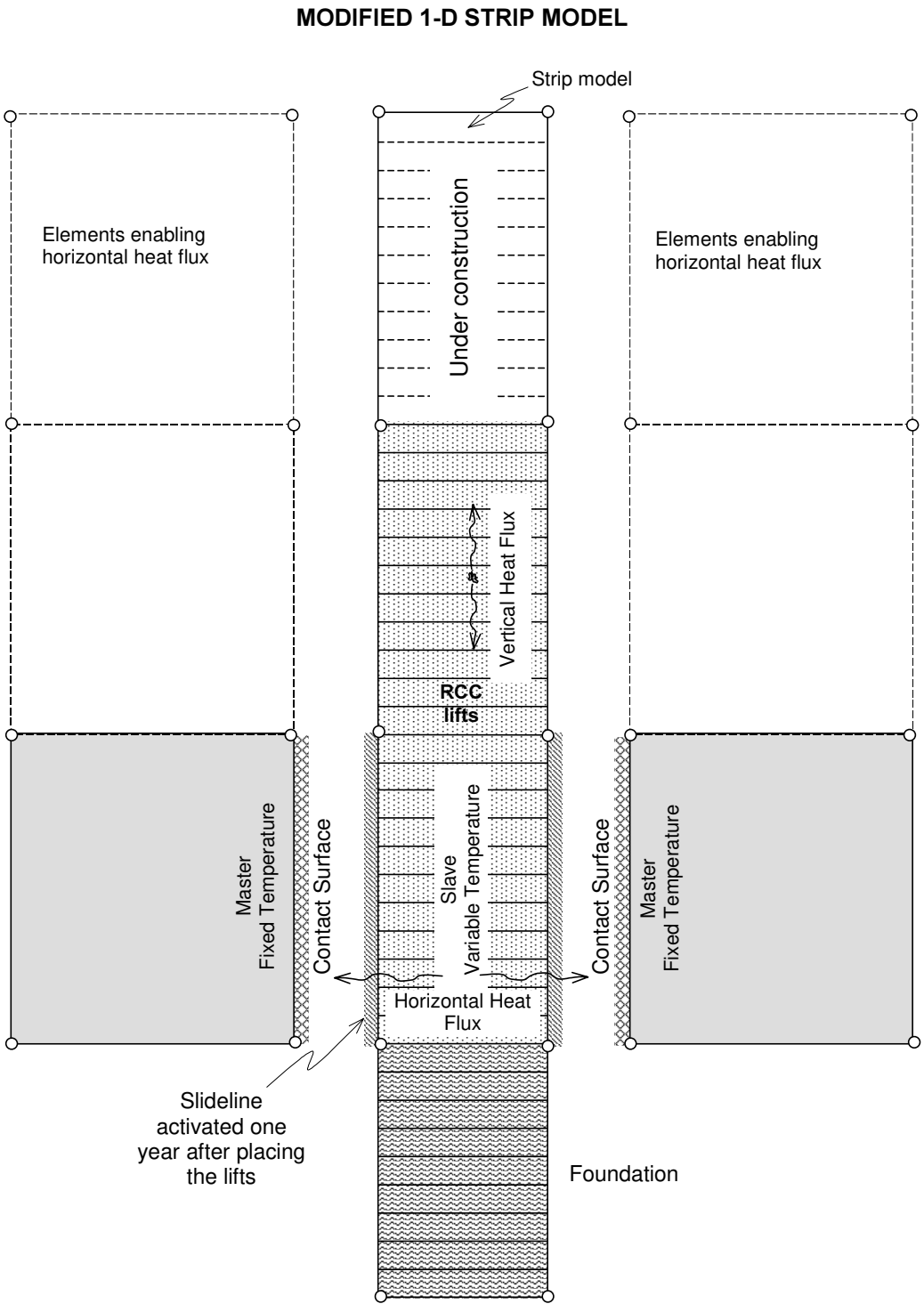

Figure 6.7: Modified 1-D strip model.

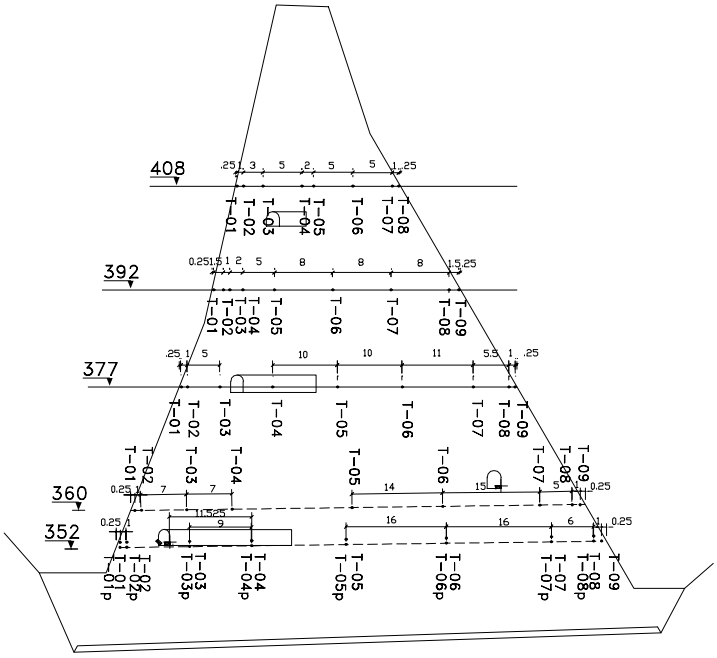

Figure 6.8: Position of the thermometers installed in block 1.

6.2.3 Initial Temperature

The activation of newly placed lifts in the model takes place at discrete points in time. This assumes that the placing operation takes place instantaneously, while in reality placement may proceed over several hours. This is one of the reasons why it is difficult to determine the initial temperature. Strictly speaking, the initial temperature comprises various different phenomena. Among these are the actual ambient temperature during placement operation, temperature of the aggregates, and temperature changes due to manipulation operations performed during the production process. Because of the complexity of this effect it is almost impossible to consider all the different influences. On the other hand, it is not always necessary to regard all the influences since some compensate each other. For instance, in areas without extreme daily temperature variation, it is not necessary to regard the variation in temperature between day and night, since setting the ambient temperature equal to the monthly average temperature gives good results. (This is based on studies done by Geringer, 1995).

In the model the initial temperature of the activated elements is automatically set equal to the corresponding placing temperature. For the simulation, the placing temperature is computed by the monthly average temperature, which represents the ambient condition, plus 2.0^oC taking into account the other phenomena. Figure 6.9 shows the average ambient

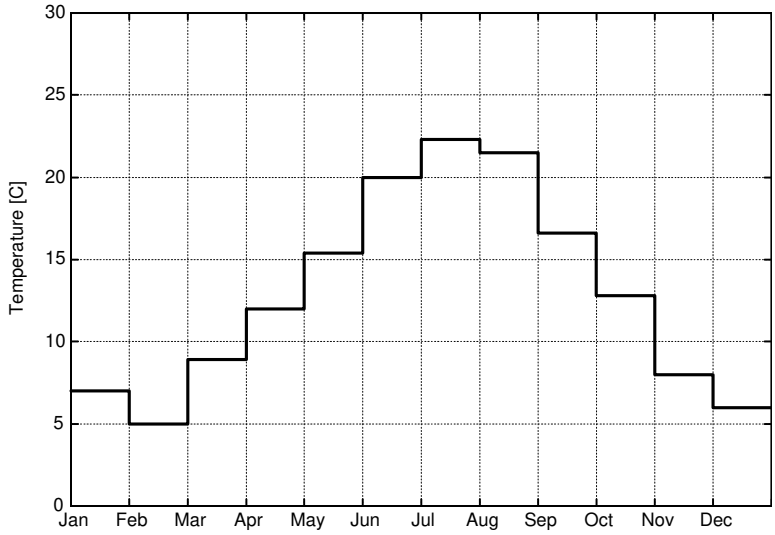

Figure 6.9: Monthly average temperature of 1996 registrated at the dam.

temperature registered at the dam during 1996.

6.2.4 Boundary Conditions at the Top Layer

To simulate the phenomenon of convection during the construction of the dam, the temperature at the surface nodes of the lift in contact with the air is automatically set equal to the placing temperature (ambient temperature plus 2.0^oC). In order to consider the effect of solar radiation, 2.0^oC are added to the upper nodes of a group of lifts placed in the months from September to May, and 4.5^oC are added to the upper nodes of a group placed during the summer months (June, July and August). Figure 6.10 illustrate the boundary conditions used for the evolutionary model.

Figure 6.11 shows the influence of the different assumptions for the boundary conditions. Graph (a) is computed considering only the ambient temperature. Note that this assumption underestimates the measured temperature in about 2.8^oC. On the other hand graph (d), that is calculated by setting the initial temperature equal to ambient temperature and assuming that there is no heat loss at the surface during construction, overestimates the measured temperature in about 7.0^oC. For graph (b) the nodal temperature is set equal to the ambient temperature plus 2.0^oC and for graph (c) the effects of solar radiation are considered. It should be noted that agreement between the model predictions of case (c) and real measured temperatures is remarkable.

A more adequate method to simulate the phenomena of convection is to place a slideline at the top of each lift, which is allowed to cool over a longer

case	T_{ini}	T_{rad}	
		Summer (Jun/Jul/Aug)	September to May
a)	T_{amb}	$0°C$	$0°C$
b)	$T_{amb} + 2°C$	$0°C$	$0°C$
c)	$T_{amb} + 2°C$	$4.5°C$	$2.0°C$
d)	T_{amb}	ISOLATED[1]	

T_{amb} - Ambient Temperature – monthly average temperature.
T_{rad} - Temperature applied in the last lift of the group.

[1] - The temperature is not prescribed.

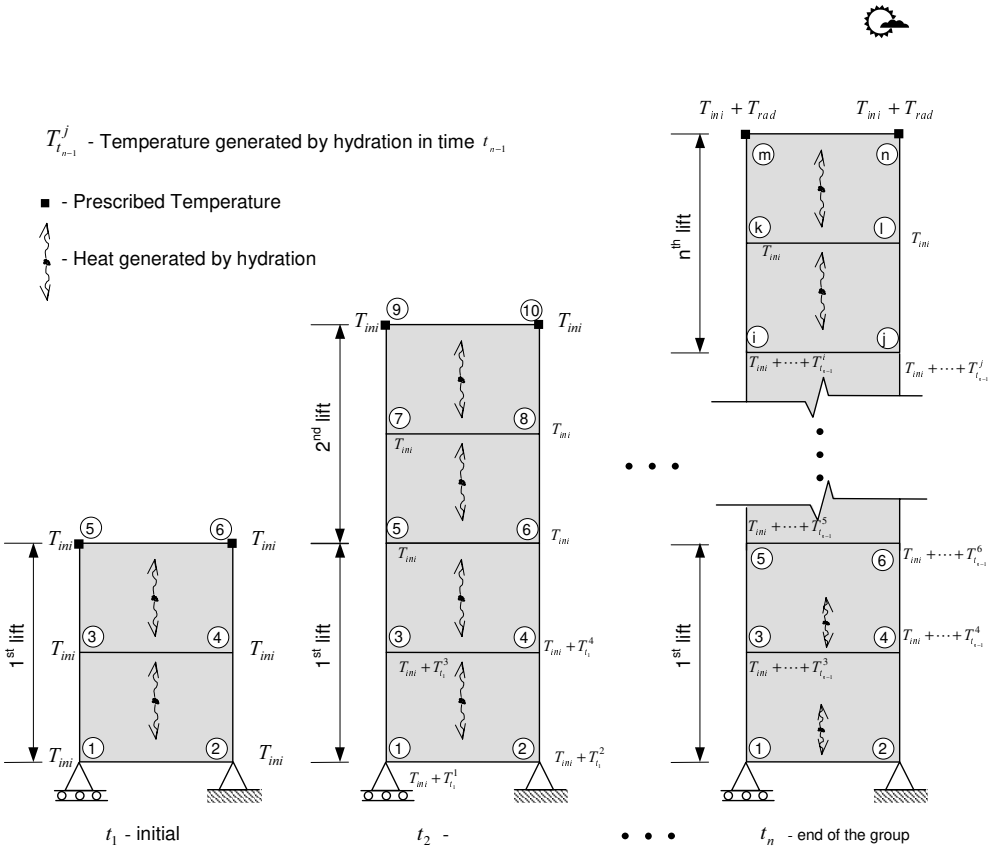

Figure 6.10: Boundary conditions of the model.

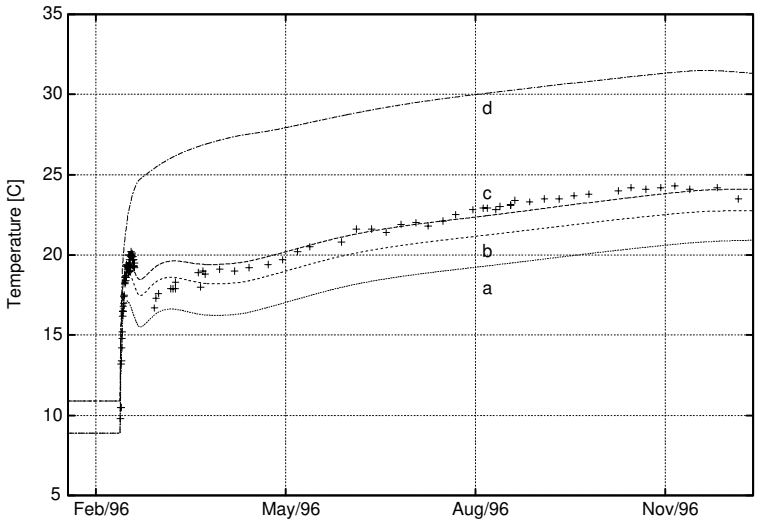

Figure 6.11: Evolution of temperature for different initial temperatures and different boundary conditions.

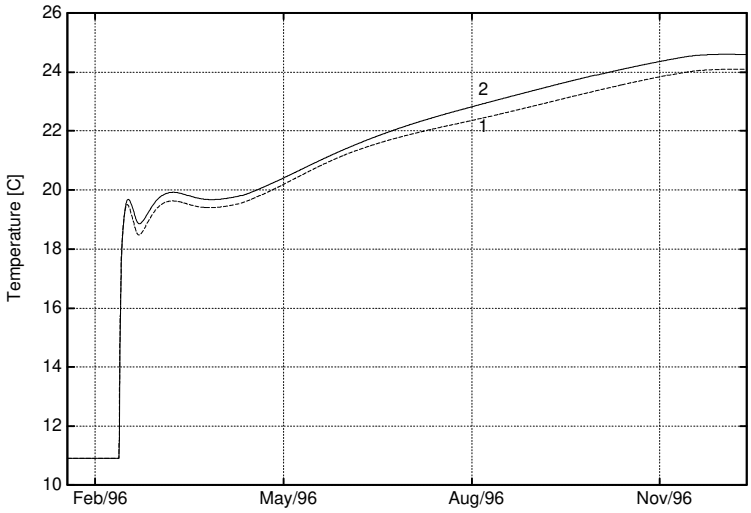

Figure 6.12: Comparison of the different models consindering the surface phenomena.

period of time. Due to the non uniform construction process the computational cost of this method is high. Hence, the strategy described above is preferred for the simulation of the reference case. Figure 6.12 compares the two different strategies. Note that, the model using the convection lines (graph 2) gives almost the same results as the model used for the analysis (graph 1).

6.2.5 Thermal analysis

The temperature distribution in a RCC dam is basically a two dimensional problem. Because of the dimensions, there is no significant heat flux in the longitudinal direction.

Construction phase

The Figure 6.13 compares the computed temperature evolution for two points, located at Elevations 352 m and 360 m, with actual in situ temperature measurements. The continuous line represents the prediction by the model and the asterisks the values obtained from the thermometers. Both thermometers are situated in the center of the dam body, about 40 m away from the upstream face in case of the thermometer 352-05, and 34.5 m in case of the thermometer 360-05.

In case of the thermometer 352-05 10 lifts are placed consecutively within 3 days in December 1995. During placement operations of these lifts the temperature reached 19^oC, this means a temperature rise of about 12^oC. After that, concreting was interrupted for 34 days. Within this time the temperature decreased 2.5^oC due to heat dissipation by convection. Following that, the temperature rises continuously, basically caused by two effects:

1. The lifts placed above work as a heat insulation, and the temperature of these lifts is slightly higher due to a higher initial temperature in January.

2. The generation of heat caused by hydration and pozzolanic reaction of the concrete lasts more than one year.

The progression of temperature of the thermometer 360-05 is a little different. The thermometer is situated in a lift constructed in the beginning of March 1996. Here 7 lifts are placed consecutively in 3 days. After reaching a first peak of about 20^oC, the temperature goes back to 16.5^oC. The temperature starts increasing again when concreting the next lifts after an interval of 5 days. Note that, even though the model is not able to reproduce

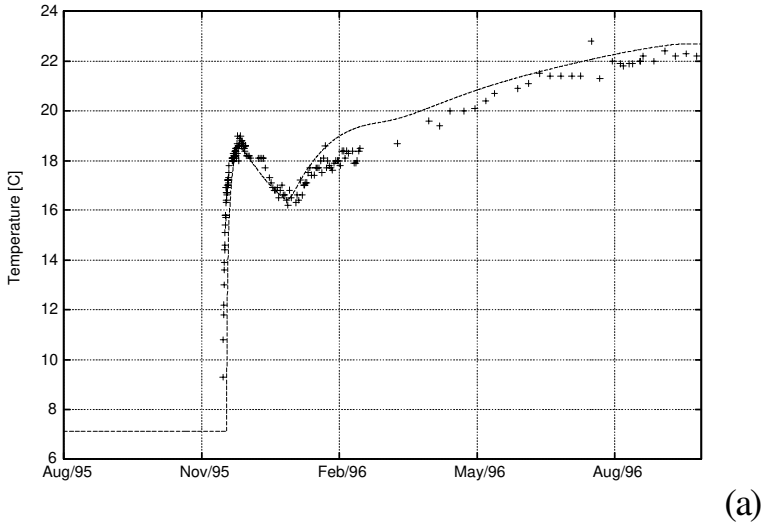

Figure 6.13: Thermometers: (a) 352-05, (b) 360-05.

exactly the evolution of temperature in the first month after placement, the overall prediction is quite good. The temperature drop, which can not be simulated by the model is caused by local phenomena such as temperatures below the monthly average temperature and elevated heat dissipation due to high humidity.

In the case of the thermometer 392-06 (January 1998), see Figure 6.14 (a), only 4 lifts were placed consecutively. Therefore the temperature rise during the first days is smaller in comparison to 352-05. On the other hand the final reached temperature is 25^oC, that is 2.5^oC higher than the maximum temperature of 352-05. That can be due to an elevated construction process during the following months. Another reason for that is that, after the break from September 1996 until February 1997, the mixture of the RCC changed. From February 1997 on, a different fly ash was used.

The thermal behavior of the lifts placed in the summer is different. The thermometer 408-05 (Figure 6.14 (b)) shows the evolution of temperature of a lift placed in June 1998. Here, the temperature reaches a peak of 35^oC 6 days after placing the 4 lifts. In the following 3 months the temperature drops down to 31^oC. After that, it starts rising again. It is remarkable that the variation of the measurements is greater than that of the previous mentioned thermometers. It is not possible to reproduce the progression of temperature during the first month by the model, using the simplified data. Possible reasons for this are:

1. This lifts and the next lifts were placed during a period of very hot weather (maximum daily temperature 32.0^oC and more).

2. The interval until placing the next lifts, indicated by the thermometer, is different from the data of the construction schedule. This means, that there can be an error in the copy of the construction schedule, or some protection was placed on top of the lift to avoid drying due to the hot weather, which had an insulating effect.

Nevertheless it should be noted that the agreement between the model prediction and the real measured temperatures is remarkable.

Operation phase

As mentioned before, usual 1-D models are not able to reproduce the long term behavior of the dam, due to the fact that they cannot simulate the horizontal heat flux. The modified 1-D model used here copes this problem by activating the slide lines (placed at both sides of the strip) when the core of the dam starts to cool down. The models permits to vary the time of activation as well as the period of time until the final temperature is

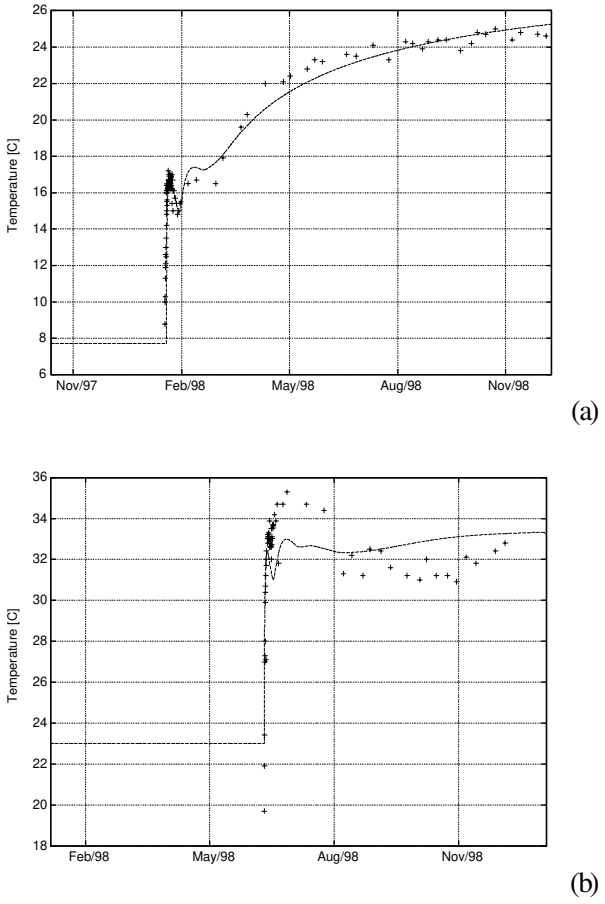

Figure 6.14: Thermometers: (a) 392-06, (b) 408-05.

obtained. Also it gives the option of replacing the final temperature with a stable temperature cycle.

The Figures 6.15 and 6.16 show the temperature plots of the long term simulation. Here it is supposed that the core reaches a final stable temperature of 14.8^oC, which is 2.0^oC higher then the average annual temperature of the last 20 years.

In the case of elevations 352 m and 360 m (Figure 6.15) the cooling of the core starts in January 1997, due to water flowing through a gallery, which is located in block 1. Since it is difficult to simulate this phenomenon in a 2-D model (Garcia Soriano, 2000), the manageability of the 1-D model allows to capture the problem without greater efforts. The velocity of cooling is adapted by variation of h (value of convection-heat-transfer) to the data measured by the thermometers. The final stable temperature is reached about 17 years after placing the concrete. Indeed, most of the cooling take place during the first three years after cooling has started.

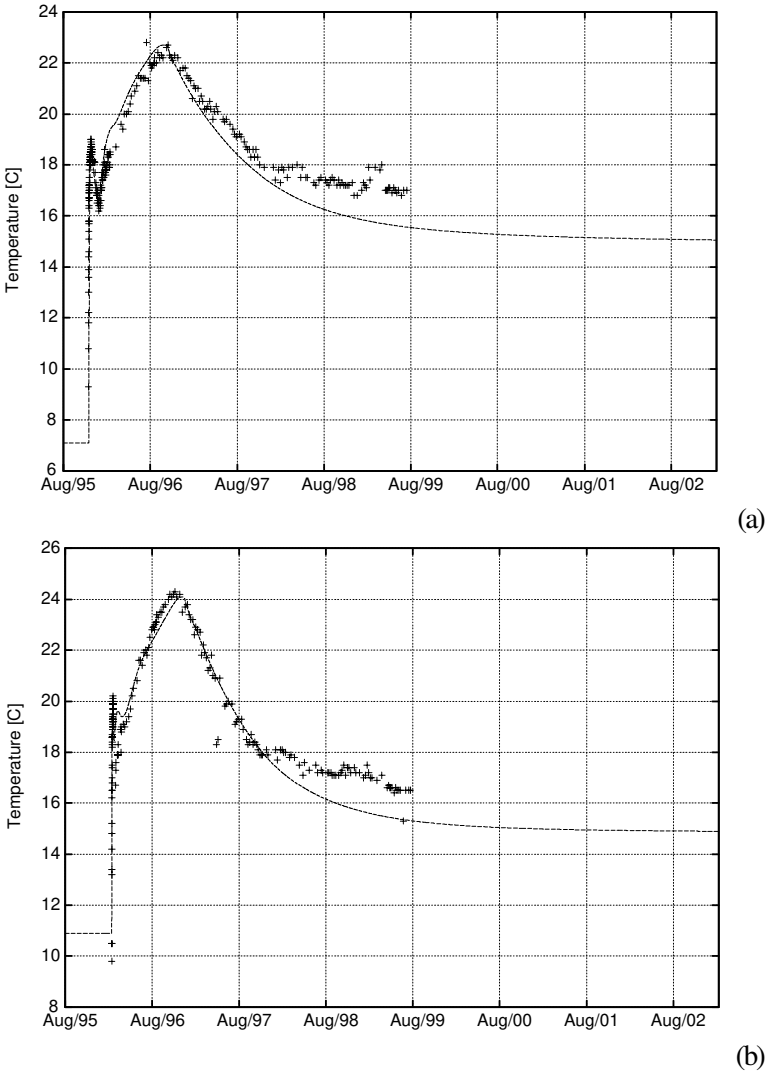

Figure 6.15: Evolution of temperature in the long term. (a) elevation 352 m, (b) elevation 360 m.

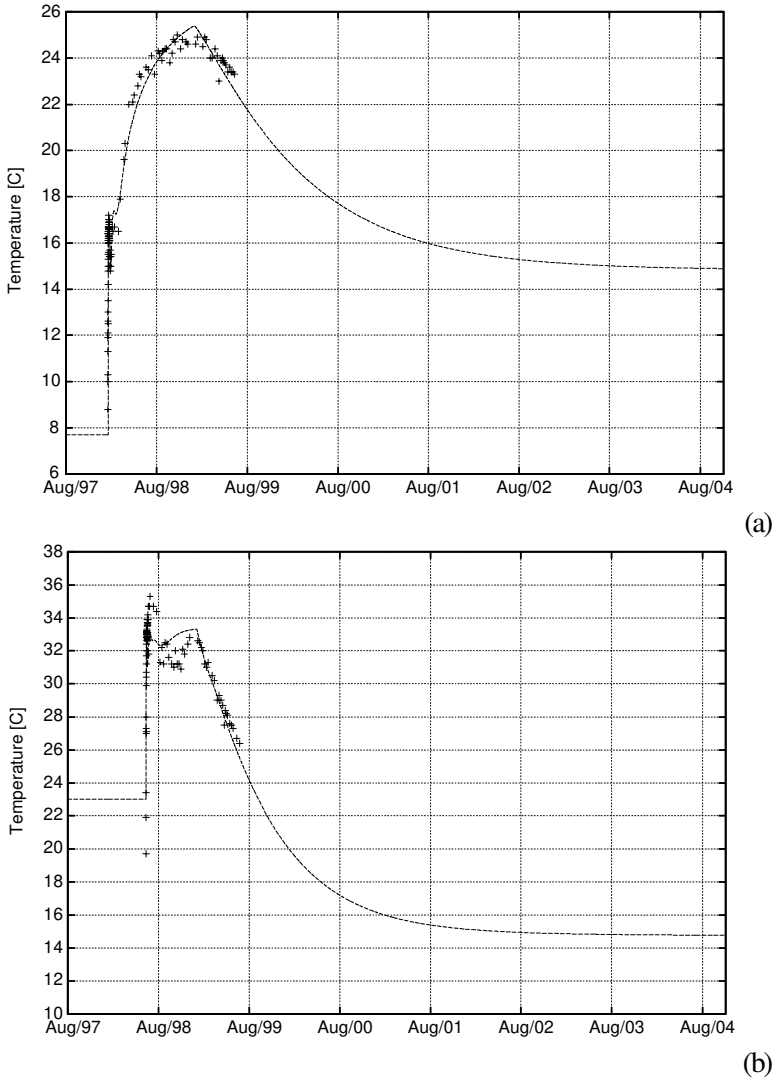

Figure 6.16: Evolution of temperature in the long term. (a) elevation 392 m, (b) elevation 408 m.

Properties	HC-1
w/c	0.41
N	2
$E^1 : E^2$	3 : 1
τ^1 $[h]$	∞
τ^2 $[h]$	15.00
$\tau_{\mu 0}$ $[h]$	600.0
$c_{\mu 0}$ $[10^{-3}$ $1/h]$	5.40
r_e^+	1.00
r_p^+	1.00
$G_{f\infty}^+$ $[N/m]$	500.0

Table 6.5: Material properties for the mechanical simulation.

In the case of elevations 392 m and 408 m (Figure 6.16) the cooling of the core starts in January 1999. While the velocity of cooling ($h = 200$ J/m^2) used for the elevation 408 m is equal to the above mentioned elevations, that of elevation 392 m is smaller ($h = 100$ J/m^2). This can be due to the greater thickness compared to elevation 408 m and the absence of interfering effects, such as galleries.

6.2.6 Mechanical Analysis

As mentioned before, thermally induced stresses have to be properly considered in RCC dam construction. A mechanical analysis provides the assessment of the dam design and the actual short and long-term safety conditions of the construction.

The mechanical analysis of the Rialb RCC dam is based on the thermal analysis described in section 6.2.5. The additional mechanical properties shown in Table 6.5 are used. They are necessary for the simulation of creep and damage. The values of the input parameters of the Maxwell-chain $E^1 : E^2$ and τ^2 have been selected based on (Schaumann, 2001). In this reference the range of admissible values corresponding to a given temperature was studied.

Figure 6.17 shows the evolution of the longitudinal stress (σ_{zz}) for interior points located at different elevations during construction. The corresponding elevations (placing months) are 352 m (December 1995), 360 m (March 1996), 371 m (September 1996), 377 m (July 1997), 392 m (January 1998), 408 m (July 1998). In general, all the are initially under compression due to the first temperature rise. During the interval until the next group of lifts is placed, compression decreases and in some cases the lifts undergo tension. After that, in the lifts placed during the cold season (352 m, 360 m, and 392 m) and with regular construction activities, compression increases,

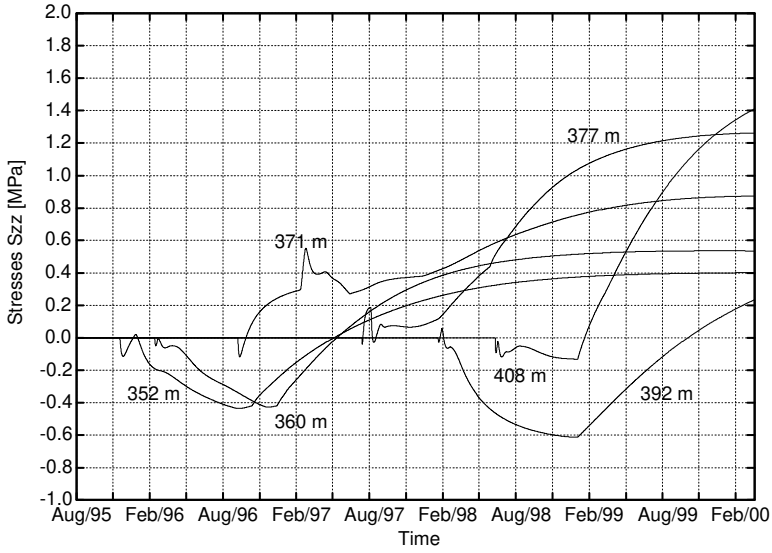

Figure 6.17: Short-term stress evolution for different elevations.

as the concrete starts to warm again because of the release of hydration heat and the heat flux coming from the surrounding concrete. This lasts until the concrete begins to cool again after the hydration is finished and the heat in the dam is released toward the environment. Elevation 371 m shows the influence on the development of stress when construction stopped from October 1996 until the end of February 1997. Due to the long time, the last lift of this group was exposed to the ambient temperature and a low initial temperature of the next placed lift, considerable tensile stresses were produced at early age. Elevation 377 m and 408 m display the evolution of the stresses of lifts placed during the summer months. In both cases the stresses remain relatively constant (tensile stress for elevation 377 m and compression for elevation 408 m) until cooling of the core starts.

Figure 6.18 shows the long-term stress evolution for the same interior points monitored in Figure 6.17. The stress analysis was run for 15 years, including the time of construction. Once the cooling of the core has started the tensile stresses increased quite rapidly. It is evident that the tensile stresses reached in the lifts placed during the summer are higher than in the lifts placed during the winter. Roughly speaking, the greater the difference of maximal reached temperature and the final stable temperature, the higher the tensile stresses attained. Indeed, the evolution of the stresses depends on various different factors. For instance, the maximum temperature of elevation 392 m is 25^oC and 24^oC for elevation 360 m. Also the maximum value of the tensile stress is almost the same. However, the maximum temperature of the elevation 352 m is 23^oC, that is the same temperature

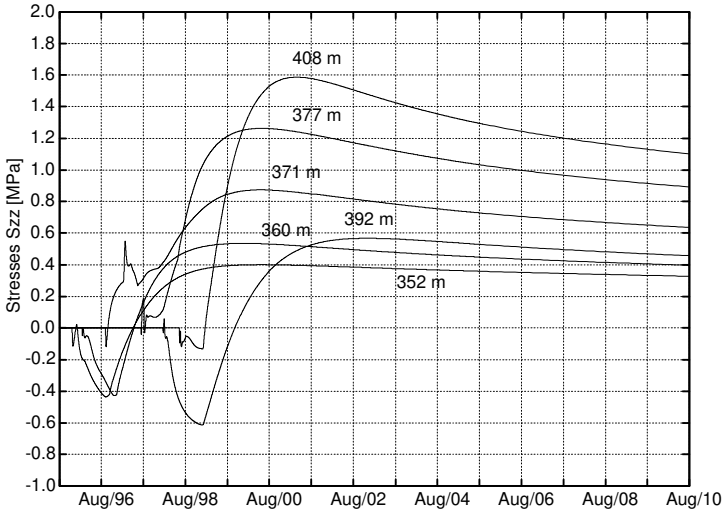

Figure 6.18: Long-term stress evolution for different elevations.

rise, but in this case a significant difference is observed in the tensile stress.

One of the factors which has great influence on the stress development is the viscous behavior of the concrete which also depends on the temperature. Figure 6.19 shows the influence of the different viscous effects considered in the model (see Section 5.2.2) on the evolution of stresses of elevation 371 m. While the Maxwell-chain considers the viscous behavior at early ages and in the mid term, the flow element has great influence on the development of stresses in the long term. Note that the final value of the tensile stress obtained in the simulation considering the viscous effects is a third of the value of the calculation which does not include the viscous effects. The loss of stress due to creep is well known. For instance the CP 110 recommends that for long term loading (duration of load $= \infty$, age at loading ≥ 100 days) the modulus of elasticity of concrete should be taken as $E_c(long\ term) = E_c/3$.

The evolution of the long term tensile stresses must be compared with the development of the tensile strength, in order to assess the risk of cracking. Note that different tensile strengths are attained at the different elevations, due to the influence of temperature in the aging process. Figure 6.20 combines both results by showing the evolution of the tensile ratio, defined as the ratio of (the norm of) the tensile stresses over the current tensile strength (Cervera *et al.,* 2000b *)*. The closer this value is to unity, the greater is the risk of the onset of tensile damage. The present analysis shows that there is no significant risk of cracking in any elevation. Higher values are obtained for the lifts placed in summer and for elevation 371 m, due to the construction stop, but they are still far away from unity.

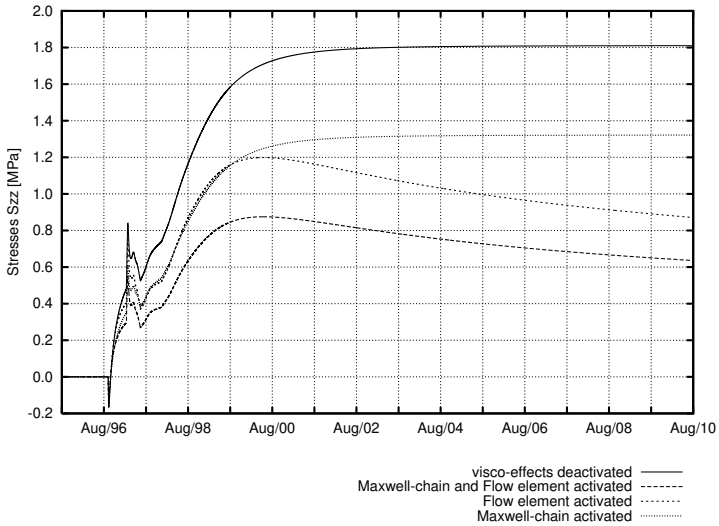

Figure 6.19: Influence of the viscous effects on the development of tensile stresses.

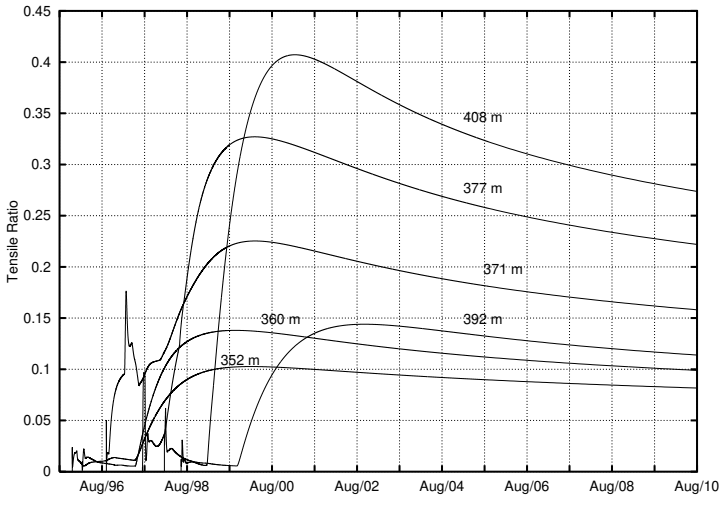

Figure 6.20: Long-term tensile ratio evolution.

6.3 Construction within 12 Months

One of the advantages of RCC dam construction is that the costs of a project can be reduced by shortened construction time due to the high concrete placement rates.

At Beni Haroun dam (Algeria), 1,600,000 m^3 of RCC (82 kg/m^3 cement, 143 kg/m^3 fly ash, which is similar to the RCC at Rialb dam) were placed within 20 months, despite the extreme climatic conditions at the site. This fact indicates that placement of the RCC at the Rialb dam could have been completed within 12 months.

In this section, results from the thermo-mechanical analysis of Rialb dam, using the fictitious construction time of 12 months, are presented. The obtained results are compared with the evolution of stresses of the reference case (see section 6.2) in order to evaluate the risk of cracking of a shortened construction time.

6.3.1 Construction Process

In order to complete placement of the RCC within 12 months, it is assumed that 8 lifts of 30 cm are placed consecutively during two days. Following that, there is an interval of 8 days until placement of the next lifts is done. This manner of construction produces a cold joint every 2.40 m. Like in the reference case construction of the dam body starts in October 1995.

6.3.2 Numerical Model

The numerical model is basically the same used for the simulation of the reference case. However to simulate the phenomenon of convection, slidelines are place a the top of each group of lifts. These slidelines are activated during the interval of time between two successive groups of lifts. As a consequence of the use of the slidelines, smaller time-steps are necessary. Normally time steps of 3 hours are used during the construction phase. During the intervals in which the convection lines are activated, time steps of 1 hour have to be used. It is one of the reasons why this method increases the CPU time considerably.

As in the reference case, the initial temperature is set equal to placing temperature of the concrete (ambient temperature + 2.0^oC). The temperature prescribed for the convection lines is the actual ambient temperature during their activation. As solar radiation is considered, 2.5^oC were added to the ambient temperature during the summer months (June, July, August) and 1.0^oC during the other months.

The slidelines which permit the horizontal heat flux are activated 1 year after the corresponding lifts has been placed. It is assumed that the core reaches a final stable temperature of 14.8^oC

6.3.3 Thermal Analysis

Figure 6.21(a) shows the temperature evolution for interior points corresponding to lifts placed with 1-month intervals between them. The corresponding (placing months) elevations are as follows: (10) 346 m, (11) 353 m, (12) 360 m, (1) 370 m, (2) 378 m, (3) 387 m, (4) 394 m, (5) 401 m, (6) 408 m, (7) 416 m, (8) 421 m, (9) 423 m. The bottom layers start to cool before the slide lines which are placed at both sides of the column are activated, due to vertical heat flow towards the foundation. Due to the higher initial temperature, maximum temperatures are obtained in the lifts placed during the summer months. Caused by heat flux towards the environment the top layers start to cool shortly after being placed. Note that the cooling rate due to horizontal heat flux are similar to the cooling rate of the top layers caused by vertical heat flux. Due to the uniform construction process all the lifts, except for the crest and the lifts close to the foundation, show similar behavior.

Figure 6.21(b) shows the long-term temperature evolution of the following elevations: 346 m (October), 370 m (January), 394 m (April), 416 m (July) 425 m (September). As in the reference case, most of the cooling takes place during the first 5 years. After that, only small changes in temperature occur until the final stable temperature is reached.

6.3.4 Mechanical Analysis

Figure 6.22(a) shows the long-term stress evolution of the above points. The stress analysis was run for 10 years, including the construction time of the dam. The reduced construction time of 12 months produces tensile stresses slightly higher than in the reference case. As in the reference case maximum tensile stresses are obtained for the lifts placed during the summer months. Regarding the month of placement, the evolution of stress has to be compared with the reference case (Figure 6.18) as follows: 370 m with 392 m, and 416 m with 408 m. The behavior of the lifts placed in January (elevations, 370 m and 392 m) is similar. Both turned into tension during the interval until the next lifts were placed. Since maximum compression for elevation 392 m is higher, the maximum value of tensile stress is almost the same. In case of elevation 416 m and elevation 408 m, which were placed during the summer months the behavior is different. Both compression and tensile stresses are higher for elevation 416 m. However, it should be stressed

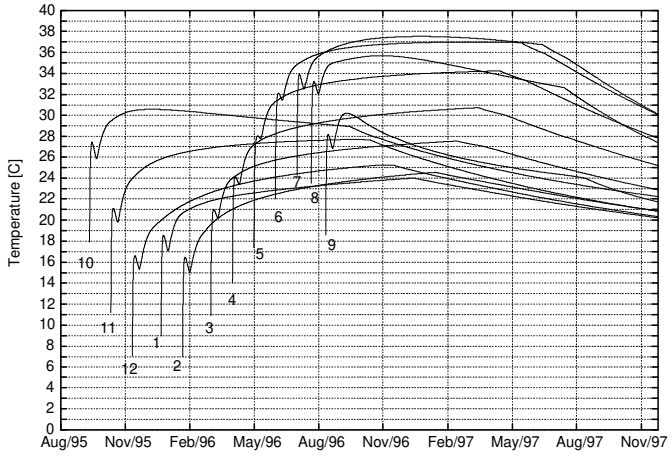

(a)

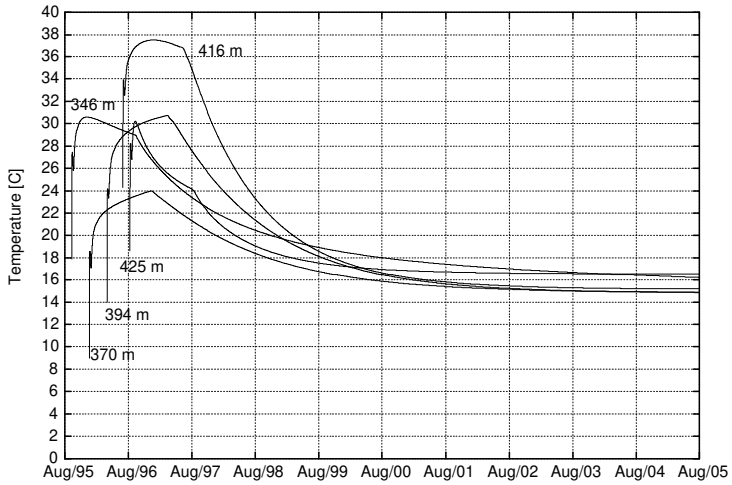

(b)

Figure 6.21: (a)Temperature evolution for different elevations. (b) Long-term temperature evolution for different elevations.

that about 72 lifts are placed during the months June, July and August in order to complete RCC placement within 12 months, which results in tensile stresses 0.3 MPa greater than in the reference case, where only 32 lifts were placed in the same period of time.

Figure 6.22(b) shows the long term evolution of the tensile ration of the above mentioned interior points. This has to be compared with the Figure 6.20 to evaluate the influence of the shorter construction time. Since the risk of cracking has decreased during the construction phase due to the uniform construction process, the maximum values are higher. As expected, the maximum value for tensile ratio is obtained for elevation 416 m. In spite of the elevated placement rate, there is no significant risk of cracking.

6.3.5 Influence of Starting Date

Despite their simplicity, 1-D strip models can be very useful to perform parametric studies on the influence of the major variables in the construction process that may affect the final temperature distribution inside the dam and at an extremely low cost.

To investigate the influence of the starting date for concreting, four different cases are compared: (1) Starting in October; (2) starting in January; (3) starting in April; (4) starting in July.

Figure 6.23 shows the comparison between the computed vertical distribution of the maximum temperatures reached in the dam body for the four cases. For case (1) the highest temperatures are obtained in the upper part of the dam. Even though the maximum temperature close to the foundation is still high, this is the most favorable case due to the fact that the difference between the highest and the lowest temperature is smaller compared to case (2). As contraction joints have been constructed over the full height of the dam this problem should not cause cracking. For case (3) the highest temperatures are obtained in the lower part of the dam. External restraint is still high at this part of the dam, so that starting construction in April can require smaller distances between the contraction joints. Case (4), starting in July, is probably the worst case, as peak temperatures are attained close to the foundation where highest restraint is provided.

Note that maximum temperatures of the four cases are very similar. That shows that they mainly depend on the placing and ambient temperatures, and on the heat release during the hydration process. However, minimum temperature vary from one case to the other, as heat flow towards the environment decreases the temperature at the crest. Similar phenomena take place at the lower part of the dam due to heat flow towards the foundation.

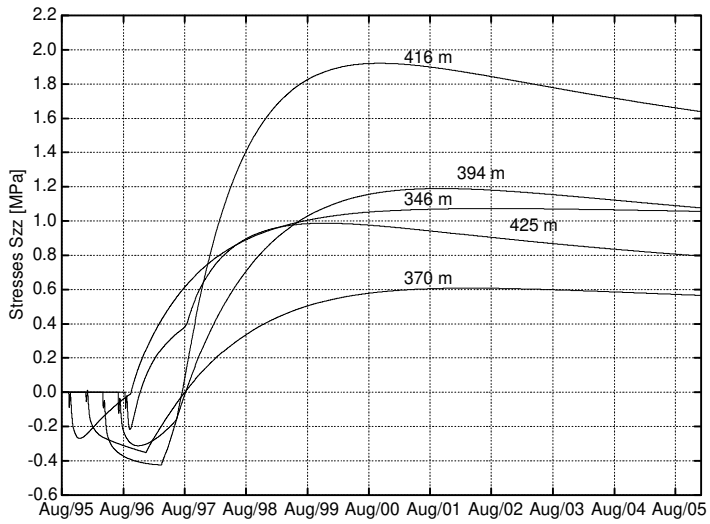

Figure 6.22: (a) Long-term stress evolution for different elevations. (b) Long-term tensile ratio evolution for different elevations.

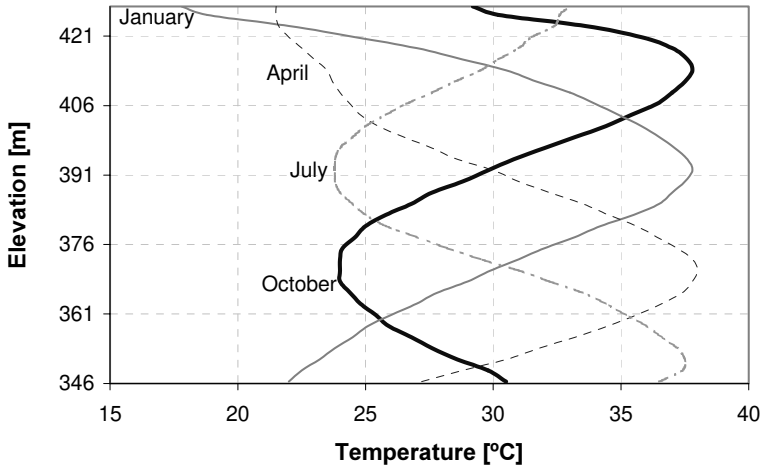

Figure 6.23: Influence of starting date.

Chapter 7

Conclusion

This diploma thesis deals with the numerical simulation of the evolution of temperature and stresses during and after the construction of RCC dams by means of a modified 1-D model. The aim of the work is to verify the prediction of temperature and stress evolution of the finite element program COMET including the constitutive model, developed by Cervera *et al.* (1999) using 1-D models. It includes the analysis of the Rialb RCC dam during and after its construction. The simulation of Rialb dam is performed using the actual conditions for ambient temperatures, placing schedules, and material properties. The obtained results are compared with the temperatures measured in the dam during the time of construction. Further methodologies to determine the initial temperature and to prescribe the boundary conditions of the evolutionary model are studied.

The following conclusions can be extracted from this work:

1. The proposed procedure is able to accurately predict the evolution of temperature due to the hydration heat production. This permits to calculate the temperature field in the core of a dam at any time during the construction process. By means of the slidelines which are placed at both sides of the strip model, horizontal heat flux can be simulated. Therefore it is possible to compute the temperature fields during the years following the completion of the dam, while the temperature in the dam body decreases to reach a final stable distribution.

2. The proposed 1-D model is able to predict the evolution in time of thermally induced stresses that develop due to hydration heat released during the construction time and the subsequent cooling of the dam body to a final stable temperature. This allows also to assess the risk of thermally induced cracking either at short or long term.

3. The constitutive model developed by Cervera *et al.* (1999) is able to predict the viscous behavior of RCC in the long term. The values

obtained in the simulation coincide with international standards and experimental results for conventional concrete.

4. Two methodologies are presented to simulate the phenomenon of convection. Both options give similar results. The method using slidelines which are placed at the top of each group of lifts and activated during the following placing interval is more accurate, but considerably time consuming. Particularly, due to the fact that it requires smaller time steps than commonly used during the construction process. Less time consuming is the methodology that prescribes the temperature in the upper nodes of the evolutionary model during the placing interval. The temperature which is prescribed in the nodes has to be determined using the method mentioned above.

5. The initial temperature for the simulation is set equal to the concrete placement temperature. The comparison of simulation results with temperature data measured at the Rialb RCC dam has shown that taking the placement temperature as the monthly average temperature + 2.0 ^oC adjusts the evolution of temperature better than placement temperatures which are calculated using the U.S.ACE model.

6. The proposed model is used to simulate the construction process of Rialb RCC dam. The evolution of temperature during the construction process is studied and the obtained results are compared with temperature data measured at the Rialb dam. Further, the simulation includes the period of time following the completion of the dam, while the core of the dam cools down to a final stable temperature. The evolution of thermally induced stresses during and after its construction is studied and assessments about the risk of cracking are made.

7. The evolution of temperature is strongly influenced by the placing and ambient temperature, the duration of placing intervals and the hydration heat generated by the concrete mix. In the simulation of Rialb RCC dam higher temperature rises are obtained in the lifts placed during the summer months; lifts placed during a period of time with decreased placing intervals also show higher temperature rises than lifts of the same initial temperature which are placed following a slower construction process.

8. The simulation shows that higher tensile stresses are attained in the lifts placed during the summer months. However, there is no elevated risk of cracking.

9. An alternative placing schedule with completion of the Rialb RCC dam in 12 months was also considered. It turns out that maximum temperatures and maximum tensile stresses are slightly higher than in the simulation of the actual construction process. But again there is no significant risk of cracking due to thermally induced stresses.

10. Long placing interval increase the risk of cracking during the construction process, but decrease the maximum value of tensile stresses during the operation phase of the dam.

11. For the simulation of the construction process it was necessary to use small time steps in order to guarantee convergence of the program. For this reason a quite simple 1-D model can become considerably time consuming. Therefore it should be investigated if the tight tolerance criteria of the program can be eased without loosing quality of the results.

12. The current preprocessor for COMET does not facilitate the input of the data necessary to simulate the evolutionary construction process. All the data required to perform the thermo-mechanical analysis have to be input manually. This manner of data input is quite laborious and fault-prone. An adequate preprocessor should be developed in order to make the simulation more user friendly.

Bibliography

ACI Committee 207.2R-90 (1990). Effect of restraint, volume change, and reinforcement of cracking of massive concrete. *J. ACI.*

Aguado, A. and Agulló, L. (1991). Analísis de las causas de daño en presas y canales españoles. In Colegio de Ingenieros de Caminos, Canales y Puertos., editor, *Actas de Jornadas sobre Reperaracíon de Obras Hidraulícas de Hormigón. E.T.S.C.C.P. Barcelona*, pages 11–50. Madrid.

Bazant, Z. and Prasannan, S. (1989). Solidification theory for concrete creep. i: Formulation. *J. Engng. Mech., ASCE*, 115:1691–1703.

Carlson, R. (1937). A simple method for the computation of temperature in concrete structures. *ACI J.*, 34:89–102.

Carol, I. and Bazant, Z. (1993). Viscoelasticity with aging caused by solidification of non aging constituent. *J. Engng. Mech., ASCE*, 119:2252–2269.

Cervera, M., Oliver, J., and Prato, T. (1999a). A thermo-chemical-mechanical model for concrete. I: Hydration and aging. *J. Engnr. Mech., ASCE*, 125:1018–1027.

Cervera, M., Oliver, J., and Prato, T. (1999b). A thermo-chemical-mechanical model for concrete. II: Damage and creep. *J. Engnr. Mech., ASCE*, 125:1028–1039.

Cervera, M., Oliver, J., and Prato, T. (2000a). Simulation of construction of RCC dams I: Temperature and aging. *J. Struct. Engnr., ASCE*, 126:1053–1061.

Cervera, M., Oliver, J., and Prato, T. (2000b). Simulation of construction of RCC dams II: Stress and damage. *J. Struct. Engnr., ASCE*, 126:1062–1068.

CP 110 (1972). Code of practice for the structural use of concrete. *British Standards Institution*.

Dunstan, M. (1988). Wither roller compacted concrete for dam construction. In ASCE, editor, *Proceedings, Roller Compacted Concrete II Conference*, pages 294–308. New York.

Dunstan, M. (1989). Recent developments in roller-compacted concrete dam construction. *Water Power and Dam Construction Handbook*.

Dunstan, M. (1999). Recent developments in RCC dams. *Int. J. Hydropower and Dams*, Six:40–45.

Faria, R., Oliver, J., and Cervera, M. (1998). A strain-based plastic viscous damage modelfor massive concrete structures. *Int. J. Solids and Structures Mech., ASCE*, 35:1533–1558.

Fujisawa, T. and Nagayama, I. (1985). Cause and control of cracks by thermal stress in concrete dams. In ICOLD, editor, *Proceedings of XV Congress on Large Dams*, volume 2, pages 117–143. Lausanne.

Garcia Soriano, J. (2000). Análisis thermo-mechánico de presas de hormigón compactado. Aplicación a la presa de Rialb. Master's thesis, Universidad Politécnica de Cataluña.

Geringer, J. (1994). The evolution and development of RCC dams in South Africa. *Int. J. Hydropower and Dams*, One:35–41.

Hansen, K. (2000). Roller compacted concrete dams - Entering the 21st century in Asia.

Hansen, K. and Reinhardt, W.G., v. . ., editors (1991). *Roller Compacted Concrete Dams*. McGraw-Hill, New York.

Houghton, D. (1976). Determining tensile strain capacity of mass concrete. *ACI J.*, pages 691–700.

ICOLD (1983). Deteriotion of dams and reservoirs. examples and their analysis. In ICOLD, editor, *Proceedings of XIV Congress on Large Dams*. Paris.

Kachanov, L. (1958). Time of rupture process under creep conditions. *Izvestia Akademii Nauk, Otd Tech Nauk*, pages 26–31.

Kaplan, M. (1960). Effects of incomplete consolidation on compressive and flexural strength, ultrasonic pulse velocity, and dynamic modulus of elasticity of concrete. *ACI J.*, pages 853–867.

Londe, P. and Lino, M. (1992). The faced symmetrical hardfill dam: a new concept for RCC. *J. Water Power and Dam Construction*.

Marsellá, J. (1996). Construcción: transporte, encofrados, puesta en obra del hormigón, juntas y galerías. In IECA, editor, *Conferencias impartidas en el* III *Curso de Presas de Hormigón compactado*, pages 208–248. Madrid, Spain.

Raphael, J. (1970). The optimum gravity dams. rapid construction of concrete dams. *ASCE*.

Salete, E. (1996). Estados térmicos. In IECA, editor, *Conferencias impartidas en el* III *Curso de Presas de Hormigón compactado*, pages 75–100. Madrid, Spain.

Schaumann, E. (2001). Numerical simulation of the development of thermally induced stresses in young concrete. Master's thesis, Universidad Politécnica de Cataluña.

Schrader, E. (1999). Shear strength and lift joint quality of RCC. *Int. J. Hydropower and Dams*, Six:46–55.

Ulm, F. and Coussy, O. (1996). Strength growth as chemo-plastic hardening in early age concrete. *J. Engng. Mech., ASCE*, 122:1123–1132.

U.S. Army Corps of Engineers (U.S.ACE) (1993). Structural design using the roller-compacted concrete (RCC) construction process. In *Tech. Letter No. 1110-2-343*, Department of the army, Washington, D.C.

U.S. Army Corps of Engineers (U.S.ACE) (1994). Nonlinear incremental structural analysis of Zintel Canyon Dam. In *Tech. Letter No. 1110-2-536*, Department of the army, Washington, D.C.

U.S. Army Corps of Engineers (U.S.ACE) (1997). Thermal studies of mass concrete structures. In *Tech. Letter No. 1110-2-542*, Department of the army, Washington, D.C.

U.S. Army Corps of Engineers (U.S.ACE) (2000). Roller-compacted concrete. In *Engineer Manual No. 1110-2-2006*, Department of the army, Washington, D.C.